Stony Brook University

IODINE CYCLING IN SEDIMENTS IN THE GULF OF PAPUA

A Thesis Presented

by

Stuart Waugh

to

The Graduate School

in Partial Fulfillment of the

Requirements

for the Degree of

Master of Science

in

Marine and Atmospheric Science

Stony Brook University

August 2008

Stony Brook University

The Graduate School

Stuart Waugh

We, the thesis committee for the above candidate for the Master of Science degree, hereby recommend acceptance of this thesis.

Dr. Robert C. Aller, Thesis Advisor
Distinguished Professor
Marine Sciences Research Center

Dr. Kirk Cochran
Professor
Marine Science Research Center

Dr. Cindy Lee
Distinguished Professor
Marine Science Research Center

This thesis is accepted by the Graduate School

Lawrence Martin
Dean of the Graduate School

Abstract of the Thesis

IODINE CYCLING IN SEDIMENTS IN THE GULF OF PAPUA

by

Stuart Waugh

Master of Science

in

Marine and Atmospheric Science

Stony Brook University

2008

Distributions of solid-phase iodine and iodide in pore water are described in surficial sediments and in sediment cores taken along an onshore-offshore transect which crosses a prograding clinoform in the Gulf of Papua. A broad spectrum of depositional and diagenetic regimes controls iodine cycling on the transect. Iodine measurements in absolute terms and normalized to organic carbon (C) and nitrogen (N) are high compared with reports in other terrigenous sediments but low compared with pelagic sediments. Topset sediments on the Gulf reflect high concentrations of iodide in porewater which result from intense cycling. A strong direct relationship is documented between solid-phase I:C ratios and δ^{13} C measurements seaward along the transect.

Iodide production is calculated from measurement of (1) anoxic incubations; (2) solid-phase iodine gradients; and (3) iodide gradients in porewater. Results are broadly in agreement with other measurements of solute production from decomposition of organic matter and confirm seasonal patterns found in the Gulf by other researchers (Aller et al 2008). Relationships between iodine and organic nutrients and between iodine and metal oxides are investigated. Correlations between iodide and dissolved Fe are found in the constant ^{210}Pb zone at several near-shore sites. Elsewhere in sediments on the transect, iodine is associated with organic material.

Comparisons of the behavior of iodine in Gulf sediments are made with the findings for iodine in Amazon shelf sediments (Mackin et al 1988). Iodine measurements on the Gulf topset are similar to those on the Amazon shelf. The two deltas are distinguished by substantial iodide production, high iodide concentrations in porewater and by convincing associations of iodine with Fe-oxides at some sites.

Table of Contents

LIST OF FIGURES

List of Tables

LIST OF APPENDICES

INTRODUCTION

Iodine is an essential nutrient and biogeochemically active element. Like N and P, it is intensely cycled during early diagenetic remineralization processes in sedimentary deposits. Despite its biogeochemical importance, iodine has been only minimally studied in deltaic systems, the primary depocenters for sediments on Earth. The present thesis documents and analyzes the behavior of iodine in a tropical deltaic environment: the Gulf of Papua, one of the major deltas within Oceania. The behavior of iodine in the Gulf of Papua is compared with that in the Amazon, the only other tropical delta studied to date.

Iodine is a halogen with multiple redox states (+/- 1,5 & 7). Its geochemical behavior in natural environments is determined by its speciation which occurs in multiple oxidation states and in inorganic as well as organic forms. In marine environments, the principal forms of inorganic iodine are iodate (IO_3^- oxidation state +5) and iodide (I^- oxidation state –1). Aqueous iodine generally occurs as iodide in reducing environments and as the more particle reactive iodate under oxidizing conditions.

Of the total quantity of iodine on earth about 30% occurs in the continental crust and 70% occurs in the oceanic crust (including seawater) (Table I) (Muramatsu & Wedepohl 1998). 98% of iodine in the oceanic crust occurs in sediments reflecting the accumulated impact of the element's biophillic character (Table II) (Elderfield & Truesdale 1980). In the lithosphere, iodine concentrations are found well below 100 ppb whereas in sedimentary deposits concentrations generally range from 100s of ppbs for sandstone to 100s of ppms for pelagic sediments (Muramatsu & Wedepohl 1998; Price et al., 1970; Price & Calvert 1973; Pedersen & Price 1980). Iodine is generally more concentrated in marine organic material than in terrestrial organic material. (Table II) (Muramatsu & Wedepohl 1998; Whitehead 1984).

Iodine is deposited at the surface-water interface of marine sediments by sinking organic particles. Yet most surficial marine sediments underlying oxygenated waters show higher iodine to carbon (I:C) ratios than found in phytoplankton (Table III). Oxygen in overlying waters is a necessary condition for iodine enrichment (Price & Calvert 1977; Ullman & Aller 1985). Generally, iodine depth profiles show exponentially increasing concentrations in pore water corresponding to decreasing solid-phase concentrations and decreasing I/C ratios in sediments. Taken together, these observations suggest a diagenetic cycling process whereby iodine delivered to the sediments associated with organic matter, is released into pore water as organic matter is remineralized, diffuses upward and again complexes with particles in oxic conditions near the sediment water interface. Cyclic rounds of burial, release to the pore water,

diffusion and re-association in surface oxic layers occur. To explain the iodine associations involved in this cycling process, researchers have proposed: (1) iodine reacts with organic matter (e.g., Price & Calvert 1977; Harvey 1980; Francois 1987) or (2) in terrigenous, near shore environments, iodate adsorbs to the surfaces of metal oxides (Whitehead 1973 & 1974; Ullman & Aller 1983, 1985; Mackin et al., 1988).

Associations with organic matter are thought to involve reaction with an intermediate electro-positive iodine species (e.g., hypoiodite (IO) or elemental iodine (I_2)) although researchers describe different precursory pathways by which the reaction is reached (enzymatic oxidation of iodide- Price & Calvert 1977; oxidation of iodide- Harvey (1980); reduction of iodate by humic materials- Francois (1980)). It is likely iodate sorbs to the surfaces of iron oxides preferentially to iodide.(Kodama et al., 2006; Ullman & Aller 1985). These proposed mechanisms are not mutually exclusive; however, the environmental significance of each mechanism is not established.

In addition to inorganic forms of iodine present in marine sediments and porewaters, significant fractions of iodine have been found as organo-iodine in soil (Kodama et al., 2006) and as dissolved organic iodine (D.O.I.) in estuarine waters (Schwer & Saatchi 2003). To comprehensively understand the mechanisms at work in the cycling of iodine in the upper oxic layers of sediment, associations of organic as well as inorganic forms of iodine may need to be taken in account.

Tropical deltas are transitional environments which receive terrestrial and marine organic carbon as well as heavily weathered debris from terrestrial drainage basins. They are characterized by areas where significant physical reworking of sediments and intense biogeochemical cycling occur. In addition to its multiple redox character, iodine is both biophilic and sorbs to metal oxides; further, it is characterized differently in marine and terrestrial material. Porewater iodide in a product of organic matter decomposition but it is not known to participate in authigenic mineral formation. Studying iodine cycling in sediments offers insight not only into the sources and modes of deposition but also into rates of organic matter decomposition.

The objective of the present study is to characterize iodine cycling in Gulf of Papua sediments in order to determine common features which are shared by tropical deltas generally and which may distinguish them from non-deltaic, terrigenous sediments. Thus comparisons will be draw frequently between iodine measured in Gulf sediments and those reported previously for the Amazon shelf.

To achieve the intended objective, the specific analytical goals of the study are to:

(1) describe the lateral distribution of solid-phase iodine in surficial sediments on a transect crossing the range of depositional environments in the Gulf;

(2) describe depth distributions of solid-phase iodine and iodide in pore water from kasten & piston cores both on an absolute basis and normalized to organic carbon (I:C ratio);
(3) estimate rates of dissolved iodide production from these sediments;
(4) relate iodine measurements to corresponding values for organic nutrients (solid-phase: C_{org} and N; porewater: ΣCO_2 and NH_4^+), and to dissolved Fe where appropriate; and
(5) analyze seasonal patterns.

It is the hypothesis of the present study that iodine associates with Fe-oxides in addition to marine and terrestrial organic material in deltaic environments, and that these associations change across the depositional system. This idea is tested by measuring correlations in porewater between iodide and dissolved Fe and between iodide and solutes generated from decomposition of organic matter (i.e. ΣCO_2 and NH_4^+). High correlations between iodide and dissolved Fe together with low correlations between iodide and ΣCO_2 or NH_4^+ are interpreted as evidence of solid-phase iodine associations with Fe-oxides. Conversely, low correlations between iodide and dissolved Fe together with high correlations between iodide and dissolved ΣCO_2 or NH_4^+ are interpreted as evidence of associations of iodine with organic matter in the solid-phase. Low correlations between iodide and all measured solutes may indicate multiple controls on iodide distributions.

GULF OF PAPUA & SAMPLING

The Gulf of Papua lies on the south coast of the island of New Guinea and forms an arc shape from the mainland southward to the Coral Sea; its shelf extends to ~ 150 km at its center and narrows towards its eastern and western perimeters (Fig.1). The Fly, Kikori and Purari rivers flow southwards from steep mountain ranges of the Papua highlands delivering a combined sediment load of ~156 MT/ yr to the Gulf's estuarine region and beyond (Aller et al., 2008). The dominant topographical features of the central Gulf are a prograding clinoform and, secondarily, relict, subaqueous river channels such as the Umuda Valley. Clinoforms are sigmoidal-shaped sedimentary deposits. In the Gulf of Papua, the clinoform consists of a broad, low-gradient topset whose seaward edge extends to water depths of ~25 m to ~ 40 m; a steeply sloped foreset which occurs between depths of ~ 30 m to 50 m; and a bottomset which occurs beyond depths of 50 m (Walsh et al., 2004). Although there remains uncertainty as to the ultimate disposition of sediment from the rivers entering the Gulf, approximately 65% of the sediment flux reaching the Gulf accumulates on the clinoform's

foreset and 25% accumulates in the broad topset; the remainder of the flux accumulates on mangrove beds or is exported offshore (Walsh et al., 2004).

Seafloor dynamics on the topset are primarily controlled by two seasonal climate regimes. During the NW Monsoons (January – March) when winds are calm and the seabed is relatively undisturbed, a drape of sediment (10 – 40 cm thick) accumulates unconformably over firmer, methanic sediment on the inner topset (< 15 m); during the SE Trades, stronger winds re-suspend these mobile muds which are eventually exported in episodic pulses to the foreset resulting in the clinoform progradation (Walsh et al. 2004). These fluid muds are reworked seasonally so no ^{210}Pb gradients are formed (Aller et al., 2008). Consequently, estimates of sediment accumulation rates for the topset are uncertain with ranges estimated between 0.7 to > 2.0 cm/yr. (Walsh et al., 2004; Brunskill, et al, 2006;). Sediment accumulation rates on the foreset average higher than elsewhere on the clinoform at > 1.5 cm/yr and on the bottomset average < 1 cm/yr (Walsh et al. 2004).

Suboxic, non-sulfidic diagenesis dominates the topset and inner foreset deposits where physical reworking of the upper layers continually reoxidizes sediments by periodically exposing them to oxygenated bottom waters. Sulfidic diagenesis becomes dominant in the outer foreset and bottomset deposits (Aller et al 2004). In the absence of bio-irrigation, oxygen penetrates at most to roughly 2 - 3 mm on the topset. (Aller et al., 2004). During the monsoons, CO_2 fluxes from surface sediments (upper 20 cm) average 35 –42 mmol m^{-2} d^{-1} on mangrove channel and topset sites and 10 –20 mmol m^{-2} d^{-1} on foreset and bottomset sites; while fluxes decrease by 30%during the remainder of the year (Aller et al., 2008). Physical reworking makes life difficult for macro-benthic organisms on the topset; instead the zone is dominated by microbial biomass. Conversely, macrofauna dominate on the outer foreset and bottomset (Aller et al., 2008).

Measurements were made of pore water and solid-phase sediments taken from cores collected by other researchers during five separate cruises to the Gulf which occurred during both NW monsoon and SE Trades periods from February 2003 to May 2004. Sampling procedures are described in Aller et al., (2008). Measurements concentrated on cores taken primarily from the GH transect (see Fig. 1) which runs from the Purari River delta seaward across the clinoform and secondarily from the Umuda Valley at a water depth of 18 m. The GH transect includes cores from a mangrove channel (GH1) through the inner topset (GH8 & GH14), the middle (GH25) and outer (GH35) topset, the foreset (GH50) and the bottomset (GH75).

METHODS

All solid-phase carbon, nitrogen, dissolved ΣCO_2 and $NH4^+$ measurements used to normalize iodine and iodide concentrations and production estimates were supplied by Robert Aller's lab at School of Marine & Atmospheric Sciences, Stony Brook University. Production estimates were calculated from measurements of porewater samples produced from anoxic incubations experiments previously conducted by Professor Aller's lab; methods used in these incubation experiments are described in Aller et al., (2008).

Available infrastructure was not developed sufficiently at the time of the study to allow for a comprehensive analysis of iodine redox chemistry in the oxic layers of Gulf sediments. Instead, the study takes advantage of suboxic or sulfate- reducing environments of deposits at the sites sampled (Aller et al 2008) at which inorganic iodine in pore water is likely present almost entirely in the form of iodide below a thin oxic upper surface layer. Consequently, iodine in sediment porewater is measured as iodide. A fraction of iodine present as dissolved organic iodine (DOI) may be missed. An estimate of the likely extreme maximum size of this neglected fraction may be calculated by multiplying the highest reported level of dissolved organic carbon (DOC) found by Aller et al., (2004) in Gulf porewater by the highest solute I:C ratio measured in porewater by this study. This calculation (□1 mM DOC X 5.0 mmol I/ mol C) yields DOI of 5 □M. This maximum estimate compares to a range of iodide values observed here from □1 to 80 □M.

Measurement of Porewater Iodide by Ion Chromatography

Iodide was measured by its UV absorbance using a Kratos Spectroflow 783 (and, after equipment failure, with a Applied Biosystems 785) UV detector. The wavelength of iodide's maximum absorbance was determined by measuring the absorbance spectra of sodium iodide solutions in artificial seawater on a Hewlett Packard 8452 diode array spectrophotometer. Maximum absorbance was detected at a wavelength of 226 nm. UV absorbance was measured in absorbance units (AU) as area under the identified peak.

To eliminate potentially interfering UV signals due to either dissolved organic matter or other anions present in Gulf porewater, measurements were made after separation of iodide on an Alltech Wescan Anion/R (10 uM) anion exchange column (100 X 4.6 mm) preceded by a Phenomenex Star-ion guard cartridge and a 7.5 X 4.6 mm C-18 guard column using a Dionex Corp 2000i Analytical pump. The mobile phase was 5mM $NaCLO_4$ solution; the eluent was filtered and degassed with a 0.2 micron polycarbonate filter and pumped with a flow rate of 1.6 mL/min. Eluent and standard solutions were made using distilled, de-ionized water with a pH □ 5. Sample injection volumes were at least 300 □L;

flow cell capacity was 12 μL. A RSI AD converter converted analogue signals to digital input to a PC. Peak Simple software recorded and analyzed AU readings.

To derive sample concentration values, measured sample absorbance was calibrated against lines calculated by least squares regression of absorbance readings measured for NaI solutions of known iodide concentrations. Iodide standards were prepared from reagent grade sodium iodide (NaI) standard in simplified artificial seawater the containing prevalent anions found in seawater (Cl^-, $SO4^{2-}$ & Br^-). All standards were prepared at the outset of measurements and kept in brown polyethylene bottles capped and maintained at ambient room temperature. Within the range of sample concentrations measured, absorbance measurements of sodium iodide standards were well-fitted to a straight line (R^2 > .98) and showed no indication of diminishing responsiveness at higher concentration levels. Estimates of standards showed moderately more variability at higher solute dilution levels (1:10) than at lower dilution (1:2 & 1:5). Consequently, all standards and samples were diluted only on a 1:2 basis (producing chlorinity of ≈ 26 mM). Measurements of the same set of standards showed moderate variation in absorbance readings from day-to-day; nevertheless, precision of standard and sample estimates was high for intra-day measurements (maximum standard deviation of triplicate analyses < 5%). For this reason, sample concentrations were calculated from standard curves calculated from standards measured on the same day and generally on the same chromatograph sequence as the porewater samples.

Measurement of Solid-phase Iodine by XRF

Solid-phase iodine was measured by X-ray fluorescence on a Bruker Pioneer spectrometer. Sediments from the Amazon delta which share a similar mineral composition to Gulf sediments were used as standards in order to match the matrix of the standards as closely as practicable with sample matrices. A standard curve was constructed (1) by measuring fluorescence from a set of Amazon delta samples with previously published total iodine concentrations for standard values below 50 μg/g (Mackin et al 1988) and, for standards with concentration above 50 μg/g, (2) by additions of known quantities of sodium iodine (NaI) solution to a homogenized mixture of these Amazon sediments selected for a low (< 3 ug/g) background level of solid-phase iodine. Additions of 5 ml of NaI solute were added to dry Amazon sediments (weighing approximately 3.33 g) in glass vials to create a slurry which was then oven dried overnight at approximately 80° C; the vial and dried sediment were subsequently re-washed with DW to remobilize any iodine residues on the side of the glass from salting-out and again dried thoroughly overnight at approximately 80° C.

Sediment samples were thawed (approximately 2 hours), dried overnight at 80° C, pulverized with a mortar and pestle or coffee grinder, weighed to 3.33 g (+/- 0.02 g) and pressed into pellet form. Pellets were pressed in a 20 mm die at 20+ tonne of pressure for 3 minutes using a 30 tonne pneumatic pellet press.

This procedure was tested by comparing net intensity levels of different pellet weights pressed at different pressures and found to yield optimal results.

The L β-1 emission line of the iodine atom was selected for measurement as it showed a higher net intensity versus background levels of the sediment sample matrix than did the Kα, Kβ or Lα lines.

Sediments selected for measurement included those from all short cores (upper 15 cm) along the GH transect, long cores from the topset (GH14) and outer foreset (GH50) as well as those from all piston cores sampled. Cores sampled during a variety of climate settings were measured including monsoons, SE tradewinds and transition periods (May and November). Standard deviation of triplicate measurements for 5 intervals from 2 piston cores averaged < 8%.

RESULTS & DISCUSSION

Surficial Solid-phase Iodine Concentrations

Surficial solid-phase iodine generally increases in concentration from the Fly River seaward along the GH transect (Fig. 2a & Table 4). Although the gradient is interrupted among the topset cores (Fig. 2 (b)), iodine concentrations increase across each depositional zone from the Fly River (26 μg/g) out to the bottomset (268 μg/g). To eliminate any effect from variation in sediment grain-size at different sites along the GH transect, solid-phase iodine concentrations were normalized to organic carbon. Table 4 shows I/C concentration ratios present in the upper 2cm of sediment; these ratios do not change materially if calculated from the upper 15 cm of sediment. Normalized to organic carbon, iodine concentrations continue to reflect the same increasing trend from the Fly River sequentially at each geological zone along the GH transect. Grain size is unlikely to have a material influence on the observed iodine concentration gradient.

Solid-phase iodine concentrations and I/C ratios share a similar increasing trend seaward with $\delta^{13}C$ measurements (Table 4). Lower iodine concentrations co-occur with lighter $\delta^{13}C$ (indicative of terrestrial carbon) nearshore whereas higher iodine concentrations co-occur with heavier $\delta^{13}C$ (indicative of marine carbon) offshore (Fig. 2(c)). Extrapolating the sequence to a marine endmember with a $\delta^{13}C$ value of – 20 yields an I:C ratio of $\approx$ 40.8 mg/g which is similar to I:C ratios in pelagic surficial sediments reported for the Panama Basin (39.5 mg/g; Pedersen & Price 1980),for the Barents Sea ($\approx$ 30 mg/g; Price et al.,1970),for the No. Atlantic ($\approx$ 22 – 32 mg/g; Kennedy & Elderfield 1987) but higher than those

reported for the eastern Pacific (~ 3 – 7 mg/g; Wakefield & Elderfield 1985). These measurements also strongly support the earlier observations of Muramatsu and others which show large differences in iodine content between terrestrial and marine sources (Muramatsu et al 1998; Whitehead 1984).

Despite the overall seaward gain in I:C ratios, iodine has a quantitatively different relationship to carbon on the topset than it does elsewhere on the transect (Fig. 2 (d)). The difference results from sedimentary and diagenetic regimes which distinguish the topset from the rest of the transect. The topset is characterized by high organic carbon concentrations and low I/C ratios. The low ratios may result from the larger fraction of less labile, terrestrial carbon present on the topset than in the more marine environment farther out the GH transect (Aller et al. 2008). Alternately, the low I:C ratios from the topset cores may reflect vertical mixing of younger, labile high iodine content material with older, more diagenetically processed material which has already undergone some degree of preferential loss of iodine. The surficial sediments on the topset are well mixed vertically on ^{210}Pb timescales (Aller et al 2008) and the measured I:C ratios may just reflect the average of sediments with different diagenetic ages. Solid-phase iodine concentrations measured in Gulf surficial sediments are high relative to reports from other terrigenous deposits but low relative to reports from pelagic deposits (Table 3). Iodine concentrations from surficial sediments in topset cores are also over twice as large as corresponding concentrations measured in Amazon shelf sediments (Mackin et al., (1988)).

I:C ratios from the topset cores are similar to those reported in the literature for coastal sediments (Price & Calvert 1973, Krom & Sholkovitz 1977, Ullman & Aller 1983) and for the Amazon delta (Mackin et al 1988) (Table 5). Excluding topset sediments from the dataset, iodine follows a direct, linear relationship with organic carbon from the Fly River seaward to bottomset (Fig 2(d)).Sediments from these sites do not reflect the vertical mixing found on the topset (Aller et al., 2008). A trendline fitted to a plot of iodine versus organic carbon at these sites shows a slope of 60.8 mg I/g C in surficial sediments along the transect. This seaward enrichment of iodine relative to carbon is steep in comparison with values reported for the Panama Basin (39.5 mg/g; Pedersen & Price 1980), for the Namibian outer-shelf (38.0 mg/g; Price & Calvert 1973) and for Loch Etive (16 mg/g; Malcolm & Price 1984).

To further examine the relationship between iodine and organic matter in Gulf sediments, iodine to nitrogen relationships (I:N ratios) were calculated. The concentrations of solid-phase nitrogen do not change materially along the transect so the I:N ratios are dominated by changes in iodine and show a similar spatial pattern to iodine itself (Table 4). An analysis of I:N ratios along the GH transect again shows two clusters as the I:C ratios did. Excluding the topset sites, iodine increases ~ 322 mg I for every 1 g increase in N . The relationship of iodine to nitrogen on the topset appears spatially trendless (data not shown). Solid-phase I:N ratios have been less frequently reported than I:C ratios. Harvey (1980) suggested iodine is present at a1:60 atomic ratio with nitrogen in

proposing a N-iodoamide association to explain iodine enrichment in marine sediments. Such an association would produce an average I/N weight ratio of ≈ 150 mg/g which is close to the I:N ratio found for the heavier ^{13}C bottomset and over twice the concentration found on the lighter ^{13}C topset.

Depth Profiles

Generally, solid phase iodine concentrations decrease with depth (Figs. 2(a), 3(a) & 4(a) - 4(c)) and iodide concentrations in porewater increase with depth (Figs. 6(a) & 7(a)) reflecting iodide release from sediments through diagenetic processes. The shapes of these profiles deviate to varying degrees from the exponential curves expected if the distributions resulted from a single first-order rate reaction such as describes solute production from remineralization offset by transport processes at steady-state. These deviations likely arise from non-steady state perturbations caused by seasonal, wind-driven turbulence on the topset and bio-irrigation on the foreset and bottomset.

Solid-phase Iodine. With the exceptions of GH1 and GH8, solid-phase profiles of short cores reflect steadily declining- if not exponentially decreasing- profiles with depth although the extent of iodine decrease varies widely among the sediment cores. (Fig 2(a)). The solid-phase GH8 iodine profile reflects near-uniform concentrations down the core; the GH1 core profile reflects low iodine loss relative to other cores. Each short core has constant ^{210}Pb activity (Aller et al., 2008) and reflects recent mixing relative to iodine remobilization (Fig 2(b)).

Solid-phase iodine concentrations and I:C ratios were measured in kasten cores at GH14 (topset) and GH50 (outer foreset) (Fig 3(a) & (b)) and in a piston core at GH14, GH50 and GH35 (inner foreset) (Figs. 4(a) – (c)). All profiles reflect iodine loss although the extent and rate of decrease varies among cores. Decreasing I:C ratios reflect preferential loss of iodine relative to organic carbon with depth. The iodine profiles from each GH50 core show steadily declining iodine levels; the I:C ratios in the piston core become erratic at mid-depth due to changes in organic carbon. The profiles from each GH14 core show immediate and substantial loss of iodine in the upper several intervals below which iodine concentrations and I:C ratios appear to reach a constant level at ≈ 30 PPM and 3 mg/g. The loss at the GH35 site is the smallest of the three sites and changes from one interval to the next are quite erratic.

Although iodine concentrations and I:C ratios at GH35 and GH50 do not fully reflect the extent of remineralization reached at the GH14 site, the values present at deepest intervals in the Gulf piston cores are quite similar despite different sedimentary regimes controlling remobilization at each site (i.e., sediment reworking and suboxic diagenesis at GH14 & slow sediment accumulation and sulfate reduction at GH50). The values at the GH14 approximate the iodine concentration (26 PPM) and I:C ratio (2.8 mg/g) found in surficial solid-phase sediments at the Fly River site and the coincidence raises

the possibility the Fly River concentration represents a refractory background level.

Most solid-phase iodine and I:C profiles reported in the literature show declining iodine concentrations and approximately exponentially declining I/C ratios for terrigenous deposits underlying oxygenated waters (Mud Bay, Ullman & Aller 1983; Amazon shelf, Mackin et al., 1988) and for hemipelagic or shelf sediments (Namibian Shelf, Price & Calvert 1977; Panama Basin, Pedersen & Price 1980). Iodine loss varies among sites depending on local sedimentary and diagenetic regimes but compared with non-deltaic deposits underlying oxygenated waters, the Gulf of Papua depth profiles are not distinctive.

Considering the similarities shared between sedimentary and diagenetic regimes on the Gulf topset and the Amazon shelf, the differences in solid-phase iodine concentrations and I:C ratios at depth between each area are noteworthy. Gulf topset and Amazon shelf deposits are both characterized by diagenetic regimes dominated by Fe reduction, reworking of seasonally fluid mud and similar rates of ΣCO_2 production (e.g., ΣCO_2 production in surficial sediments (< 20 cm) in inner topset sediments vary between ~ 35 – 42 mmol m^{-2} d^{-1} (Aller et al 2008) whereas average ΣCO_2 production in Amazon shelf deposits is ~ 53 +/- 16 mmol m^{-2} d^{-1} in the upper ~1-2 m (Aller et al 1996)). Yet solid-phase iodine concentrations in the kasten cores sampled in Amazon shelf sediments decrease to substantially lower levels than found at depth in the Gulf piston cores measured. For instance, the I:C ratio estimated for the GH14 topset core only reaches a background value of ~ 3 mg/g at depth sampled down to over 400 cm whereas I:C ratios in Amazon shelf sediments reach ~ 1 mg/g at depths of only 230 cm. These higher background I:C ratios in the Gulf topset sediments may derive from (1) more refractory iodine in Gulf sediments than in Amazon shelf sediments; (2) more efficient remineralization of solid-phase iodine over the entire core depth sampled in the Amazon shelf than in the Gulf topset sediments (as opposed to ΣCO_2 production rates in surficial sediments compared above); or (3) different ages of the sediment at equivalent depth intervals brought about by differences in sedimentation rates between the Amazon shelf and the Gulf topset.

Porewater Iodide. Porewater iodide profiles are reported in Fig (5) – Fig (7). The profiles reflect approximate exponential shapes over the depth-scales of piston cores (Fig. 6 (b)) at the GH14, GH35 & GH50 sites. Such curves are consistent with stead-state decomposition of organic matter. Over more shallow depth-scales and even over the 4 m depth of the piston core at the Umuda Valley site, porewater profiles are influenced by non-steady state controls (Figs. 6 (b), & 7 (b)).

Generally, iodide concentrations are higher in porewater of sediments at sites on the topset than on the foreset or bottomset. Higher sediment accumulation, sub-oxic carbon incineration or release from Fe-oxides may generate more iodide in pore waters of the topset than on the foreset or

bottomset. Increased irrigation/ bioturbation on the foreset and bottomset relative to the biologically depauperate topset area could also reduce solute concentrations in the pore water offshore relative to inshore. These explanations are not mutually exclusive and could each play a role in accounting for observed pattern.

Despite higher solid-phase iodide concentrations in surficial sediments, porewater iodide concentrations from Gulf topset cores are lower than those measured in porewater from Amazon shelf sediments. As Table 6 shows, maximum porewater iodide concentrations reached at depth from both Amazon shelf and Gulf topset deposits are more similar to each other than concentrations from non-deltaic sediments and appear to distinguish the two deltaic systems.

Iodide Profiles with Intermediate-depth Maxima & Minima. The distribution of iodide in the pore water from kasten cores from topset sites (GH8 & GH14), from GH1 (a channel in the mangroves) and from a piston core at a Umuda Valley site at a 14m water column depth share similar profiles (Figs. 6 (b) & 7(b)). Iodide profiles at these sites are characterized by a maxima occurring above a mid-depth minima both of which occur within a mobile mud zone having uniform ^{210}Pb readings (Aller et al. 2008). These minima roughly co-incide with lower layer of the mobile mud which lays unconformably above a zone of firmer and stable methanic sediment where iodide concentrations again begin to gradually increase with depth. Depths at which the maxima and minima occur vary among cores. Iodide profiles from foreset and bottomset sites do not show such shapes but instead reflect a steady increase in iodide concentrations (Fig. 6 (a)).

Formation of similarly shaped solute profiles in constant ^{210}Pb layers has previously been attributed to bio-irrigation, authigenic mineral precipitation or by nonsteady-state solute production from reactive sediments occurring over non-reactive sediments (Mackin et al 1988). There are no reports of iodide participating in authigenic mineral formation and since macrofauna are largely absent on the topset (J.Aller, et al., 2008), these profiles must owe their shape to non-steady state production. Accordingly, maxima may represent periods of slow deposition between periods of more rapid accumulation; alternately, they may reflect pulsed deposition of iodine enriched marine particles preceded and followed by deposition of particles less enriched in iodine.

Additionally, in the uniform ^{210}Pb layers of topset cores, iodide maxima roughly coincide with dissolved Fe profiles and bear little relationship to $\Sigma CO2$ profiles (Fig. 8 (a) & (b)). The co-incidence of iodide and dissolved Fe maxima are not evident in intervals below the uniform ^{210}Pb layer of topset cores nor in profiles from cores on the foreset or bottomset. Instead a more general correlation with ΣCO_2 is evident reflecting accumulation of dissolved solutes from the remineralization of organic matter (Fig. 8(c)). This difference between the solutes with which iodide correlates is also evident in correlation data (Table11). In foreset and bottomset porewater, iodide has negative correlations with

dissolved Fe and strong correlations (mostly > 0.90) with solutes produced from the decomposition of organic matter- i.e., ΣCO_2 and NH_4^+. But, at least at GH1 and at the Umuda Valley site, iodide has negative correlations with these decomposition products and high correlation with dissolved Fe. Iodide is not convincingly correlated with either dissolved Fe or with products of organic decomposition at GH8 and GH14 either during the monsoons or during the trade winds. As previously discussed, iodide concentrations in pore water are higher at topset sites than at foreset or bottomset sites; and this pattern also applies to dissolved Fe. Porewater from GH1 has the highest iodide and dissolved Fe concentrations measured on the GH transect during the monsoons. The Umuda Valley site also has high iodide and dissolved Fe concentrations.

The profiles and correlation data suggest iodide production occurs as part of the decomposition of organic matter at sites on the foreset and bottomset but occurs in the mangrove channels and topset as result of processes in which dissociation from mineral complexes and specifically from Fe-oxide also plays a role of varying importance. At GH1 and T8-18, dissociation from Fe-oxides may dominate iodide production in some depth intervals while at GH8 and GH14 mutliple processes may be involved, perhaps including both dissociation from mineral oxides and decomposition of organic matter.

Mackin et al., (1988) attributed iodide production in Amazon shelf sediments to the net release of iodine from associations with Fe-oxides by Fe reduction during sub-oxic diagenesis brought about by physical reworking of sediments. One of the primary reasons for the finding was the absence of coherent relationships between iodide and NH_4^+ in incubation experiments or in pore water solute distribution data. While the present study found evidence of coherent relationships between iodide and NH_4^+ in production and solute data across the foreset/bottomset of the GH transect, no coherent relationships were found at topset sites, consistent with the findings of Mackin et al 1988, (Fig.9). Not only did the present study find a lack of correlation between iodide and ΣCO_2 and NH_4^+ on the topset but it also demonstrated a strong correlation between increases in iodide and dissolved Fe in pore water at least at two sites: GH1 and the Umuda Valley site.

Production

Iodide production was estimated by (1) measuring iodide concentrations in porewater stored after previous anaerobic incubation experiments; and (2) calculating flux derived from concentration gradients. Incubated samples were only available in readily analyzable form for short cores. Production rates were derived from the difference between iodide concentrations in porewater of samples frozen immediately after extraction (t=0) and samples frozen after anaerobic incubation periods of from 3 – 13 days (t=1) and from 32- 37 days (t=2).

Modeling Iodide Production from Solid-phase Iodine Concentration Gradients.The flux method was only applied to cores where exponential curves could be fitted to solid-phase iodine profiles (Appendix 1 - 4). Accordingly, curves were fitted to reactive solid-phase iodine concentrations from short cores along the GH transect from GH14 to GH75. The solid-phase iodine profiles at GH1 and GH8 could not be fitted to exponential functions with $R^2 > 0.8$ and consequently production estimates for these cores were only derived from incubation data. Reactive solid-phase iodine was derived from measured distributions less an estimated non-reactive background. The exponential curves fitted to the data was of the form

$$I(z) = I_0 * EXP(-\beta * z) \quad (1)$$

where I_0 is reactive iodine concentration at z = 0 and β is a first order rate constant derived from a plot of reactive solid-phase iodine concentrations against depth. For the topset (GH14) and inner foreset (GH35) cores, production rates were then calculated at steady state; i.e.,

$$\partial I/\partial t = - \omega * (\partial I/\partial z) - R(z) = 0 \quad (2)$$

where ω is the sedimentation rate and R(z) takes the form

$$R(z) = R_0 * EXP(-\beta * z) \quad (3)$$

and R_0 equals production at z=0 (Burdige 2006). While steady state assumptions especially with regard to sediment accumulation rates are not consistent with physical reworking of topset deposits over deeper intervals, concentration gradients over the upper 15 cm fit exponential functions reasonably well for GH14 and GH35 and the production function generated a flux estimate which was within range of production estimated from direct incubation measurements.

For the outer topset (GH50) and bottomset cores (GH75), production rates in surface deposits (5 – 10 cm) were calculated at steady state with an adjustment (D_b) for the effect of particle mixing brought about through bioturbation on iodine concentrations; i.e.,

$$\partial I/\partial t = D_b * ((\partial^2 I/\partial z^2) - \omega * (\partial I/\partial z) - R(z) = 0 \quad (4)$$

where D_b is the co-efficient of particle mixing estimated from ^{234}Th excess activity measurements in these sediments. ^{234}Th mixing rates are derived from unpublished data from direct gamma counting of core samples (R. Aller, pers. com.)

Solid phase iodine production was estimated as flux (J) integrated over the 15 cm depth of the core (i.e., at steady state, net flux in/out of sediments equals production) according to the formula;.

$$J = \int R(z)\,dz \quad (5)$$

$$= (R_0/\alpha)\,(1 - EXP(-\alpha * z)) \quad (6)$$

where ϕ equals average porosity over the interval integrated.

Most of the sediment accumulation rates (ω) used to derive the production functions are given in Aller et al., (2008). Accumulation rates for the topset site (GH14) and inner foreset site (GH35) are uncertain due to the movement of fluid muds. Consequently, upper and lower boundaries for production are reported based on ranges of sediment accumulation estimated for nearby sites by Walsh (2004).

Estimates of Iodide Production in Surficial Sediments (< 15 cm). Table 7 compares values for estimated production calculated (1) from solid-phase iodine concentration gradients and (2) from incubation measurements. Production rates calculated from solid-phase gradients are generally lower than rates calculated from incubations. Such an outcome is reasonable since solid-phase iodine likely includes complexes in less labile or refractory associations whereas iodide measured in incubations is by definition from reactive material. If production equations with the higher sediment accumulation rates are used, the flux estimates for GH14 and GH35 fall in between the rates calculated from incubations. Only at the GH75 site is there a substantial incongruity between flux and incubation estimates. Cores from this site are the most heavily bioturbated of all cores taken from the GH transect (Aller et al 2008). While an effort was made to correct for the influence of particle mixing on the flux estimate, confirmation of the incubation rates was not feasible for this core.

Incubations show rates of production slowing down over the t=2 time interval from higher rates during the t=1 period except at the GH50 site. This decrease is consistent with consumption of a fixed substrate in a closed system. The t=1 result for the GH50 site is deemed suspiciously low; consequently, the flux derived from the concentration gradient is the preferable estimate in the case of GH50 but likely represents only a minimum estimate for production at the site. The estimate also matches the production rate derived from the incubation measurement at t=2. In subsequent calculations, rates of production from the t=1 incubations will be used except for the GH50 site where the flux rate derived from its concentration gradient will be used.

With the exception of the estimate for the GH1 site, production rates calculated from the iodine solid phase gradients and from iodide release during the anoxic incubations are within ranges reported in the literature for surficial sediments from other deltas and estuaries. Ullman and Aller (1985) reported J-flux valves of surficial deposits (0-10 cm) in Mud Bay, No. Carolina and in Long Island Sound of 14 and 29 mols/m^2-d respectively and Mackin et al. (1988) reported 85 mols/m^2-d from the upper 20 cm interval of sediments from Amazon delta.

Production numbers also agree with patterns of iodide concentrations in pore water at some sites (Figure 2 (a) & (b)); i.e. high rates of production at GH1 and GH8 produce high iodide concentrations in pore water and low rates at GH50 produce low porewater iodide concentrations. However, iodide production rates estimated from the t=1 incubations at GH35 and GH75 appear high relative to the low iodide concentrations in pore water at these sites. The GH75 site is heavily bio-irrigated (Aller et al., 2008); and production rates calculated from incubations in a closed system may not be reflected in solute concentrations if macro-faunal burrows allowed iodide to diffuse away to the overlying bottomwater. Thus iodide concentrations may appear low relative to iodide production because of transport conditions. X-radiographs of sediment structures along the GH transect suggest bio-irrigation may also influence results from the GH35 site (Aller et al 2008). An alternate explanation is the t=1 incubation numbers may be too high.

Regardless of whether incubation or solid phase model flux data or some combination of the two data sets is used, estimates of iodide production from the GH short cores do not show a steadily increasing seaward gradient in contrast with iodide concentration measurements. Instead a U-shaped pattern occurs with extremely high production of iodide at GH1, lower production on the topset and a unsteady increase in rates seaward across the rest of the transect (Table 7).

Table 8 compares iodide production to production of ΣCO_2 and NH_4^+. ΣCO_2 production fluxes in surficial sediments (< 15 cm) decrease seaward across the GH transect except at the GH35 site; NH_4^+ production appears erratic both on an absolute basis and relative to carbon. The GH35 site is characterized by low solid-phase concentrations but high production for iodide, ΣCO_2 and NH_4^+. I:C production ratios which reflect the production of iodide normalized to the production of ΣCO_2 are less erratic than iodide production alone (Table 8). I:C production ratios are high in the mangrove channel and inner topset, reach a low on the outer topset and increase again at the bottomset site. The U-shaped pattern reflects both differences in depositional regimes and differences in the level of iodine enrichment in source material at each site. GH1 is a rapidly accreting sediment pile entraining reactive organic debris and even a small quantity of labile material can drive high porewater production rates. On the other hand, GH75 is a slowly accreting deposit which receives a greater fraction of highly labile marine plankton highly enriched in iodine. I:N ratios show the same U-shaped pattern with relative iodide production highest on the outer bottomset/outer topset and mangrove channel/inner foreset and lowest on the outer topset/inner foreset.

I/C and I/N production ratios are all higher than one as iodine is preferentially consumed relative to organic carbon and nitrogen in these layers (incubation layer 0-15 cm). As reflected in the profiles of solid-phase I:C and I:N ratios from kasten cores and piston cores, this preferential consumption continues down core.

Comparing Production Ratios with Porewater Solute Stoichiometries. Solute stoichiometries derived from the slope of the plot of iodide against ΣCO_2 or NH_4^+ in porewater were compared against I:C and I:N production ratios (Table 10). At steady-state, solute stoichiometries should equal solute production ratios. I:N ratios were adjusted by diffusion coefficients for all cores. There was no coherent relationship between iodide and ΣCO_2 in data from the GH35 site and ratios from this site are not reported.

The solute data from the short cores yield different I:C ratios than the production data at the GH1 and GH75 sites. The disparity likely arises because GH1 and GH75 are impacted by wind-driven, vertical mixing and bio-turbation respectively; consequently, the steady state assumption does not hold at these sites. There is less of a disparity between the porewater stoichiometry and the I:C production ratios at the other sites. The I:N porewater stoichiometries are generally more closely matched to I:N production ratios except at the GH14 site raising the question of whether carbonate re-precipitation may play some role in the poor match between I:C production ratios and porewater stoichiometries. The $NH4^+$ data were corrected for adsorption and $NH4^+$ does not precipitate to form minerals under the incubation conditions. The results suggest the I:N ratio may be a better indicator of trends in the relative production of iodide compared with the decomposition of organic matter than the I:C ratio.

Modeling Iodide Production from Iodide Porewater Profiles. For pore water iodide profiles, a curve was fitted to measured iodide distributions according to

$$I(z) = I_0 + (I_{max} - I_0)(1 - EXP(-\Phi * z)) \qquad (7)$$

where I_{max} is iodide concentration at its asymptotic value; the terms I_0 is the iodide concentration at z =0 and Φ is a first order rate constant. The deeper piston cores provided more data which allowed exponential curve fits with higher R^2 than data from long and short cores for the same sites. Consequently, only data from piston cores were fitted to equation (7) (Appendices 5-7).

Production rates were then calculated at steady state by

$$\partial I/\partial t = D_s * (\partial^2 I/\partial z^2) - \omega * (\partial I/\partial z) + R(z) = 0 \qquad (8)$$

where D_s is the molecular diffusion coefficient of iodide which is calculated as D_0 at 28° C (Table 4.8; Boudreau 1997) adjusted for viscosity (Table 25; Riley 1976 and tortuosity (Berner 1980). Since all piston cores had Peclet numbers substantially greater than one, production calculations for piston cores include the advection term. R(z) is again defined as

$$R(z) = R_0 * EXP(-\Phi * z) \qquad (9)$$

where R_0 equals production at z=0.

As with solid-phase estimates, production from iodide concentrations in pore water was estimated as flux (J) integrated over the depth of the core (i.e., at steady state, net flux in/out of sediments equals production).

Estimates of Iodide Production from Piston Cores. Iodide production was estimated from iodide gradient in pore water from piston cores on the topset (GH14), inner foreset (GH35) and bottomset (GH50) (Table 9). Rate constants amongst the profiles were similar (range -.0073 to -.0086) and very close to published rate constants for sulfate consumption for the piston core (-.0084) and CO_2 production (-.0112) for the long core at the GH50 site (Aller et al 2008). Flux numbers are substantially lower for piston cores (1-3 mols/m^2-d) than for short cores reflecting the drop in production rate as iodide approaches an asymptotic value at deeper intervals. The low production rates over the depth-scales of the piston cores are consistent with the high terminal solid-phase iodine concentration levels noted in the discussion on iodine depth profiles.

A Comparison of Seasonality on the Topset and Foreset

Long cores were taken on the topset at the GH14 site during monsoon (February 2003), at the end of the NE trade winds (November 2003) and again at the start of the subsequent monsoon (January 2004). Comparing the iodine profiles in solid-phase and pore water from each period offers a picture of how changing physical/climate forces impact the geochemistry of the sediments on the topset. Solid-phase depth profiles (Fig. 10 (a) & (c)) show what appears as a pulse of iodine at the GH14 site in the November 2003 sample (end of the tradewinds period) which wasn't apparent in the February 2003 sample (middle of the monsoon period). While progradation of the clinoform occurs with net movement of sediment from rivers to the foreset and beyond (Walsh 2004), the increase in iodide in the upper 40 cm of sediment at GH14 from monsoons to trades periods suggests the deposition- at least temporarily- of iodine enriched offshore sediments. This received pulse of iodine is reflected in higher iodide concentrations in the pore water in November (Figure 10 (c)). By January 2004, the additional solid phase iodine has disappeared from the sediment. It is unclear to what degree the loss reflects diagenetic processes versus physical removal or exchange of sediment.

Neither solid-phase iodine nor porewater iodide concentrations offer any evidence of such climate forces on the outer foreset (Fig.10 (b) & (d)). Although the upper two layers of the solid-phase long cores cross, data points in solid-phase and solute depth profiles almost overlap in cores taken at GH50 in the monsoons (January 2003) and during SE trade winds (September 2003).

Iodide production in the upper 15 cm at the GH14 site in November 2003 decreases to 0.7 of its monsoon level (Table 13). This decrease agrees with

estimates of ΣCO_2 production for surficial sediments over the entire topset between monsoon and trade period (Aller et al 2008). The decrease in $NH4^+$ production over the period at the GH14 site is much greater than those decrease in ΣCO_2 over the same period and is not readily explainable. Iodide production at the GH50 site increases only slightly over the period and agrees with measurements of ΣCO_2 and $NH4^+$ production.

The age of the seasonally variable drape of mud at GH14 the length of which was estimated by Aller et al (2008) at a maximum of ~40 cm thick can be estimated based on iodide production. Assuming (1) production remains roughly constant over the deposition period and (2) sediment in the layer was deposited with a pore water composition equal to overlying bottomwater and (3) diffusive transport is negligible over the period since deposition, then

$$\Sigma I = \Sigma_{0\text{-}15} * R\, t \qquad (10)$$

where I = average iodide concentration over estimated depth of mobile mud, Φ = porosity, t = age of iodide growth and R = iodide production rate. For GH14 during the trade wind period, the above equation yields an age of 120 days. The core from the GH14 site for the trades was taken in November and 4 months earlier would place the deposition date in July or right in the middle of the SE tradewind period.

Alternately, the age of the fluid muds can be estimated based on changes in bulk, solid-phase iodine concentrations by

$$(1 - \Phi_u) * \Sigma_{sed} I_u - (1 - \Phi_b) * \Sigma_{sed} I_b = \Sigma_{0\text{-}15} * R\, t \qquad (11)$$

where I represent total solid-phase iodine concentrations at upper (u) and base (b) intervals and Σ_{sed} is sediment density. For the sediment measured at the trade winds date, the equation yields an age since deposition of 446 days.

CONCLUSIONS

Like the Amazon delta, the Gulf of Papua is a transitional environment where depositional inputs change from terrestrial to marine sources. A broad spectrum of sedimentary regimes control the cycling of nutrients on the GH transect. The GH1 site is a rapidly accreting sediment pile in a mangrove channel characterized by marine sourced ^{210}Pb (Aller et al 2008) where high iodide remobilization may reflect suboxic release of solid-phase iodine from Fe-oxides in the constant ^{210}Pb zone. Topset sites are characterized by intense physical mixing and sub-oxic diagenesis. At the GH8 & GH14 sites, iodine geochemistry

may be governed by multiple diagenetic processes with no one reaction exerting a dominant influence on iodide concentrations within the constant ^{210} Pb zone . Beneath these well mixed layers, iodide remobilization becomes more closely linked with increases in the concentrations of solutes associated with the decomposition of organic matter. Poised on the steeply sloped foreset, the GH35 site receives episodic pulses of heavily reworked sediments seasonally from the topset. The roughly uniform iodine depth profiles (both absolute and normalized to organic carbon) at the site reflect the refractory character of the depositional material. Iodine profiles at GH50 and GH75 reflect more oceanic sediment accumulation rates, control by remineralization of highly iodine- enriched organic matter and bio-irrigation. Surprisingly, iodide production estimates, both absolute and relative to ΣCO_2 and NH_4^+ , reflect highest production at either end of the clinoform but for entirely different reasons.

Seasonal climate patterns were found to impact sediment deposition as reflected in iodine distributions on the topset at GH14 but not on the outer foreset at GH50. Iodide production was found to change seasonally to the same extent as for other solutes across the Gulf (Aller et al 2008). However, high concentration of iodide in porewater immediately after the SE tradewinds are difficult to reconcile with lower solute production during the period.

Cores taken from the GH transect afford the opportunity to track changes in geochemical balances as the sedimentary environment transitions from terrestrial to marine based deposition. This study documented the correlation between surficial I:C ratios and δ^{13}C measurements of TOC in surface sediments along the transect. The relationship has not been documented in other near shore or deltaic environments and whether the correlation holds up in such settings remains an open question. A cursory examination of I:C ratios from Mackin et al 1988 and a map of δ^{13}C measurements of TOC over the Amazon shelf (Showers & Angle 1986) suggests at least a general correlation between the two indicators as each increase in a seaward direct. However, Mackin et al's data are primarily from topset deposits on the clinoform and, consequently, the I:C ratios reported are low. Whether I:C ratios from Amazon sediments in deeper water would bear out the correlation is unknown.

Based on the findings of this study and of an earlier study on deposits from the Amazon shelf (Mackin et al 1988), deltas contain topset areas of intense iodine cycling driven by suboxic diagenesis in depositional environments characterized by seasonal physical working of sediments. Iodide production in surficial sediments of the Amazon shelf was reported at 85 μmol/m^2-d (Mackin et al., 1988). The present study found iodide production at the topset GH8 site at 90 μmol/m^2-d and likely substantially higher still at GH1. These estimates underline the intensity of iodine cycling in these deltaic areas. In contrast, iodide production in surficial sediments in Long island Sound and Mud Bay were reported at 14 and 29 μmol/m^2-d. Based on evidence from the Gulf of Papua and the Amazon shelf, deltas are distinguishable from other terrigenous sediments by high level of iodide production and high concentrations of iodide in porewater as well as by

instances of associations between iodine and Fe oxides.

REFERENCES.

Aller, R.C., N.E.Blair & G.J. Brunskill (2008) Early diagenetic cycling, incineration and burial of sedimentary organic carbon in the central Gulf of Papua (Papua New Guinea). Journal of Geophysical Research 113, 1-22.

Aller, R.C., A. Hannides, C.Heilbrun & C. Panzeca (2004) Coupling of early diagenetic processes and sedimentary dynamics in tropical shelf environments: the Gulf of Papua deltaic complex. Continental Shelf Research 24, 2455-2486.

Aller, R.C., N.E. Blair, Q. Xia & P.D. Rude (1996) Remineralization rates, recycling and storage of carbon in Amazon shelf sediments. Continental Shelf Research 16 (5/6), 753-785.

Aller, J.Y. & R.C. Aller (2004) Physical disturbance creates bacterial dominance of benthic biological communities in tropical deltaic environments of the Gulf of Papua. Continental Shelf Research 24, 2395- 2416.

Alongi, D.M., P. Christoffersen, F. Tirendi, and A.I. Robertson (1992) The influence of freshwater and material export on sedimentary facies and benthic processes within the Fly Delta and adjacent Gulf of Papua (Papua New Guinea). Continental Shelf Research, 12, 287-326.

Berner, R.A. (1980) Early Diagenesis, A Theoretical Approach. 241 pp. Princeton University Press, Princeton, N.J.

Boudreau, B.P. (1997) Diagenetic Models and Their Implementation. 414 pp. Springer-Verlag, Berlin.

Brunskill, G. J., I. Zagorskis, and J. Pfitzner (2003) Geochemical mass balance for lithium, boron, and strontium in the Gulf of Papua, Papua New Guinea (Project TROPICS). Geochimica et Cosmochimica Acta, 67, 3365-3385.

Burdige, D.J. (2006) Geochemistry of Marine Sediments.609 pp. Princeton University Press, Princeton, N.J.

Elderfield,H. & V.W. Truesdale (1980). On the Biophilic Nature of Iodine in Seawater. Earth and Planetary Science Letters 50, 105-114.

Francois R. (1987a) The influence of humic substances on the geochemistry of iodine in nearshore and hemiplegaic marine sediments. Geochimica et Cosmochimica Acta 51, 2417- 2427.

Guenther, E.A., K.S. Johnson & K.H. Coale (2001). Direct ultraviolet spectrophotometric determination of total sulfide and iodide in natural waters. Analytical Chemistry 73, 3481-3487.

Harvey, G.R. (1980) A study of the chemistry of iodine and bromine in marine sediments. Marine Chemistry , 327-332.

Kennedy, H.A. & H. Elderfield (1987) Iodine diagenesis in pelagic deep-sea sediments. Geochimica et Cosmochimica Acta 51, 2489-2504.

Kodama, S., Y. Takahashi, K. Okumura, T. Uruga (2006). Speciation of iodine in solid environmental samples by iodine K-edge XANES: Application to soils and ferromanganese oxides. Science of the Total Environment 363, 275-284.

Krom, M.D. & E.R. Sholokovitz (1977) Nature and reactions of dissolved organic matter in the interstitial waters of marine sediments. Geochimica et Cosmochimica Acta 41, 1565-1573.

Mackin, J.E., R.C. Aller & W.J. Ullman (1988) The effects of iron reduction and nonsteady-state diagenesis on iodine, ammonium and boron distributions in sediments from the Amazon continental shelf. Continental Shelf Research 8 (4), 363-386.

Malcolm, S.J. & N.B. Price (1984) The Behavior of Iodine and Bromine in Estuarine Surface Sediments. Marine Chemistry 15, 263-271.

Muramatsu, Y. & K.H. Wedepohl (1998) The distribution of iodine in the earth's crust. Chemical Geology 147, 201-216.

Pedersen, T.F. & N.B. Price (1980) The geochemistry of iodine and bromine in sediments of the Panama Basin. Journal of Marine Research 38, 397-411.

Price, N.B. & S.E. Calvert (1973) The geochemistry of iodine in oxidized and reduced recent marine sediments. Geochimica et Cosmochimica Acta. 37, 2149-2158.

Price, N.B. & S.E. Calvert (1977) The contrasting geochemical behaviors of iodine and bromine in recent sediments from the Namibian shelf. Geochimica et Cosmochimica Acta. 41, 1769-1775.

Price, N.B., S.E. Calvert & P.G. W. Jones (1970) The distribution of iodine and bromine in recent sediments of the southwestern Barents sea. Journal of Marine Research 28, 22-34.

Riley, J.P. & G. Skirrow (1975) () Chemical Oceanography, 2nd ed. Vol 1. Academic Press, London.

Schwehr, K.A. & P.H. Santschi (2003) Sensitive determination of iodine species, including organo-iodine, for freshwater and seawater samples using high performance liquid chromatography and spectrophotometric detection. Analytica Chimica Acta 482, 59-71.

Shower, W.J. & D.G. Angle (1986) Stable isotopic characterization of organic carbon accumulation on the Amazon continental shelf. Continental Shelf Research 6 227-244.

Ullman, W.J. & R.C. Aller (1983) Rates of iodinde remineralization in terrigenous near-shore sediments. Geochimica et Cosmochimica Acta 47, 1423-1432.

Ullman, W.J. & R.C. Aller (1985) The geochemistry of iodine in near-shore carbonate sediments. Geochimica et Cosmochimica Acta 49, 967-978.

Wakefield S.J. & H. Elderfield (1985) Interstitial water iodine enrichments in sediments from the eastern Pacific. Journal of Marine Research 43, 951-961.

Walsh, J.P., C.A. Nittrouer, C.M. Palinkas, A.S. Ogston, R.W. Sternberg & G.J. Brunskill (2004) Clinoform mechanics in the Gulf of Papua, New Guinea. Continetal Shelf Research 24 (19), 2487-2510.

Whitehead, D.C (1973) The sorption of Iodide by soils as influenced by equilibrium conditions and soil properties. J. Sci. Fd Agric. 24, 547-556.

Whitehead, D.C (1974) The sorption of Iodide by soil components. J. Sci. Fd Agric, 25, 73-79.

Whitehead, D.C. (1984) The distribution and transformations of iodine in the environment. Environmental International 10, 321-339.

Figures

Tables

&

Appendices

Fig. 1 Map of the Gulf of Papua (Aller et al., 1988)

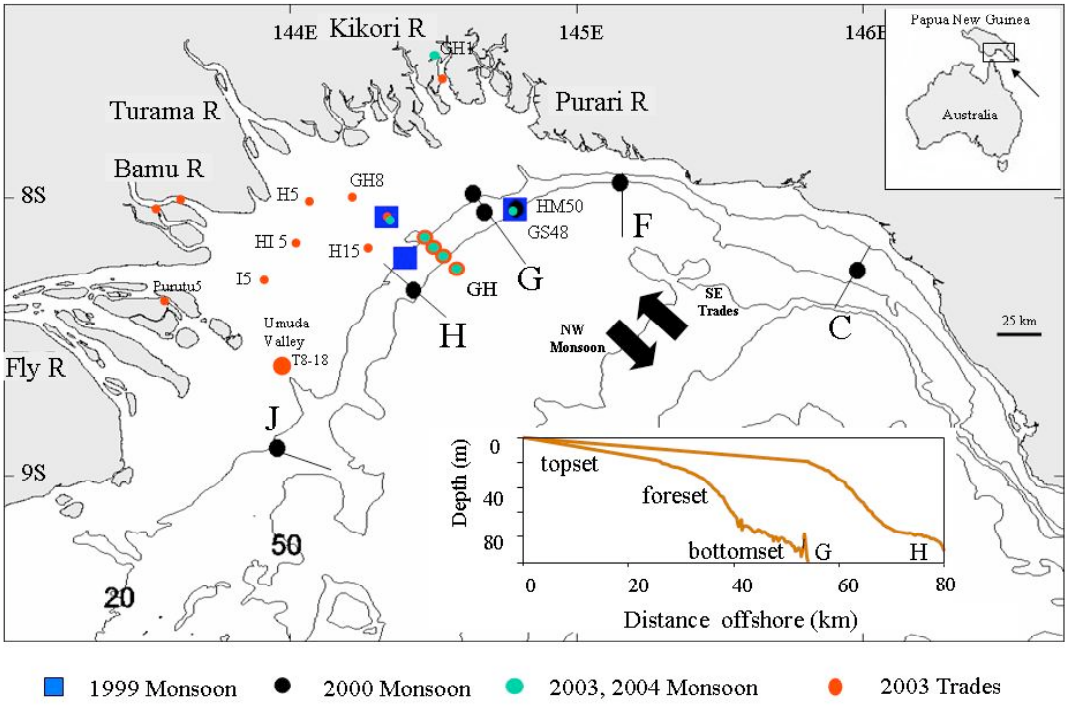

Fig. 2 (a). Depth profiles of solid-phase iodine from short cores on GH transect (Sediments sampled in 2003 monsoons except for GH35 in Nov 2003).

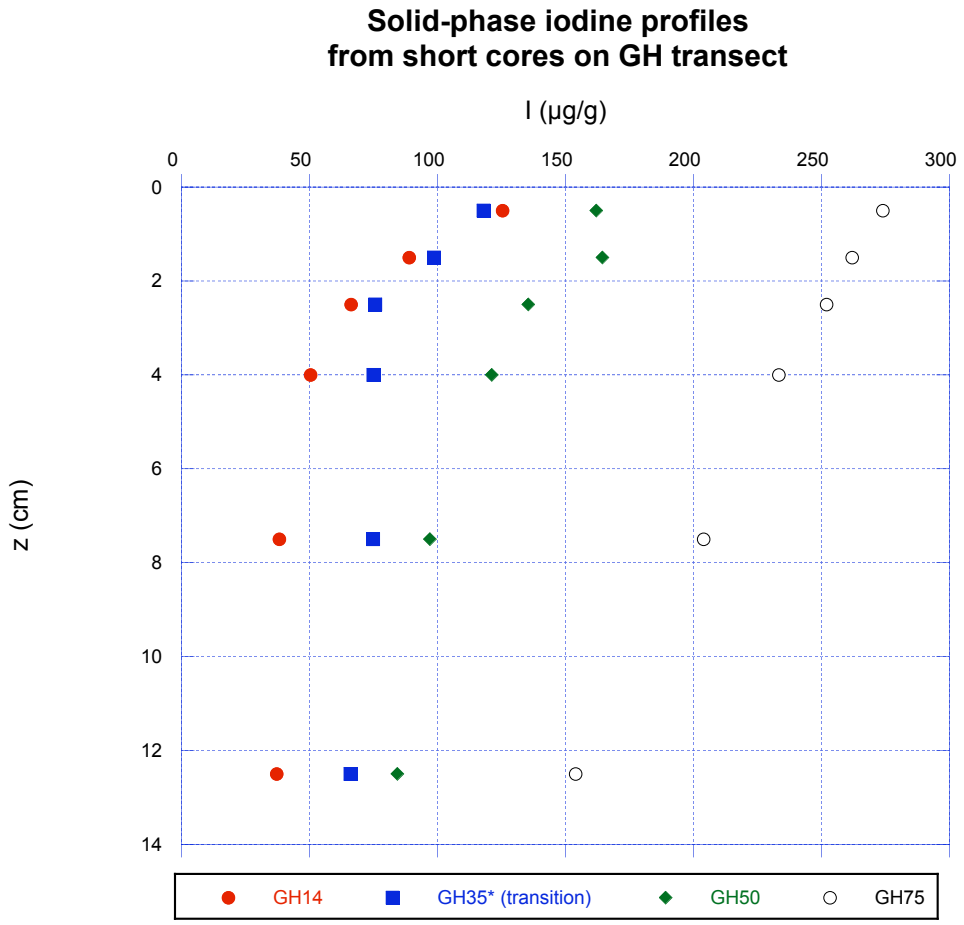

Fig. 2(b). Depth profiles of solid-phase iodine from short cores from topset deposits. Sampled 2003 monsoon except GH8 Nov 2003.

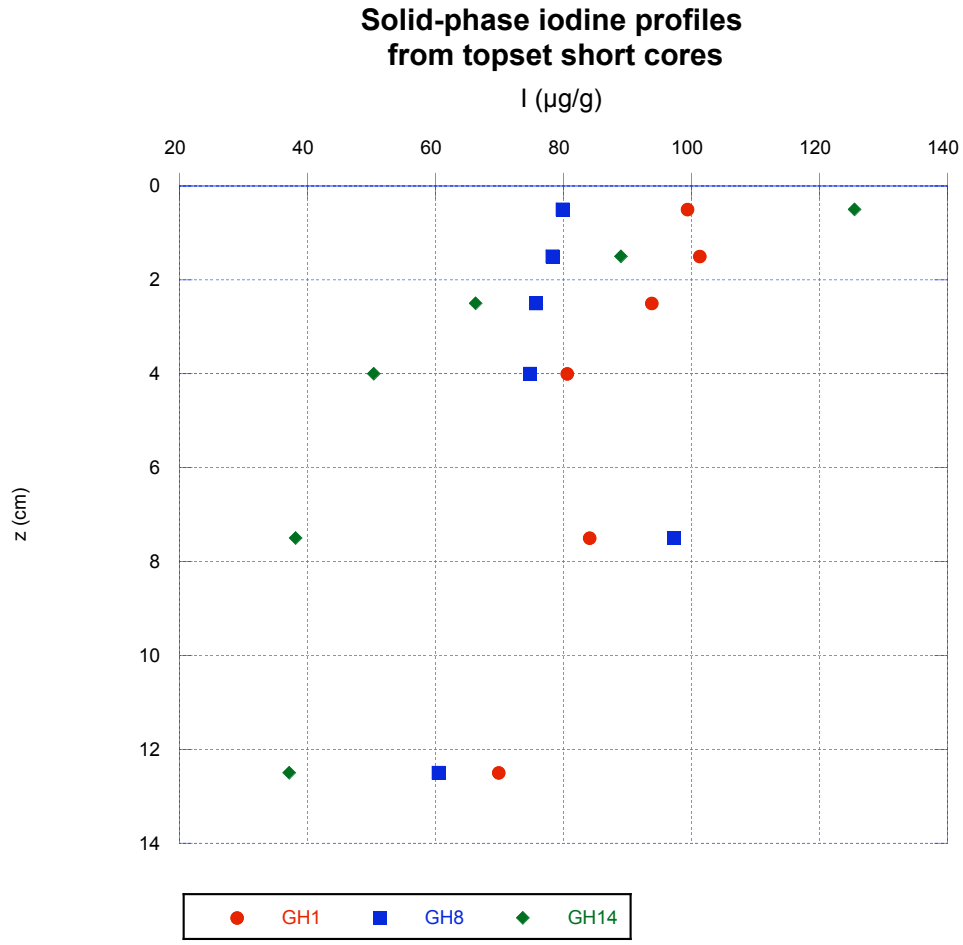

Figure 2 (c). Solid-phase I:C ratios regressed against $\delta^{13}C$ values at sites along the GH transect.

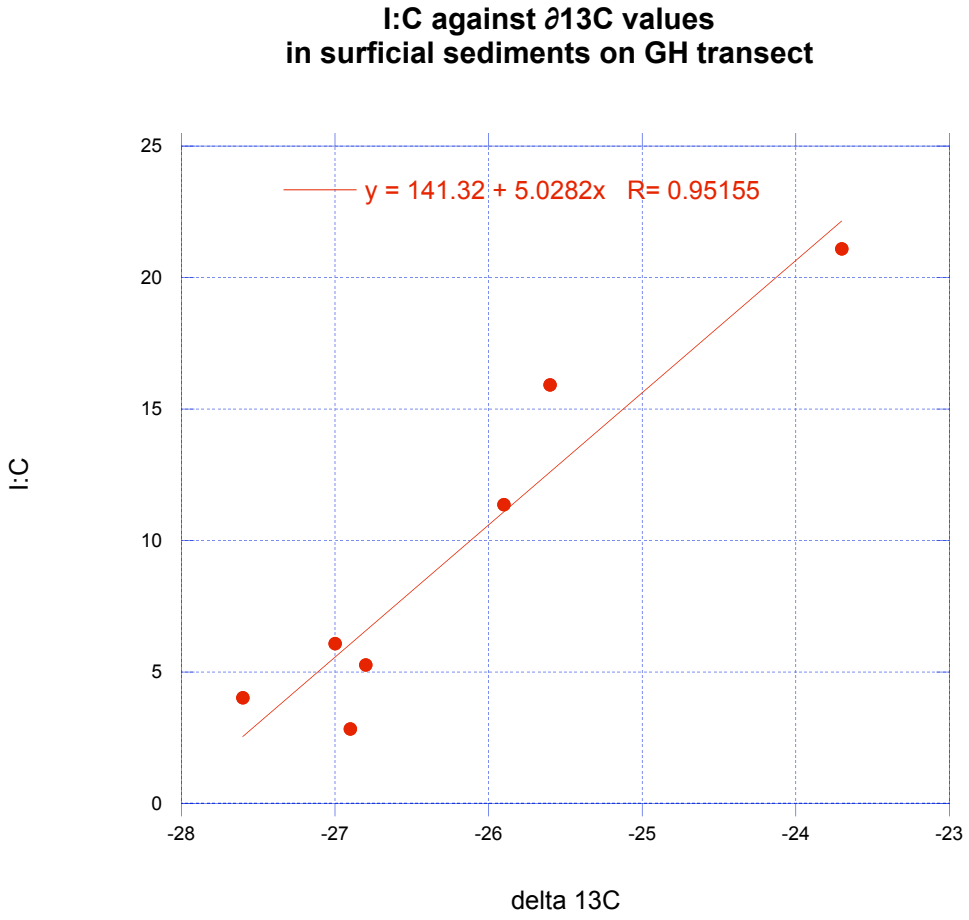

2 (d). Iodine: Carbon Gradients on GH Transect in surficial sediments

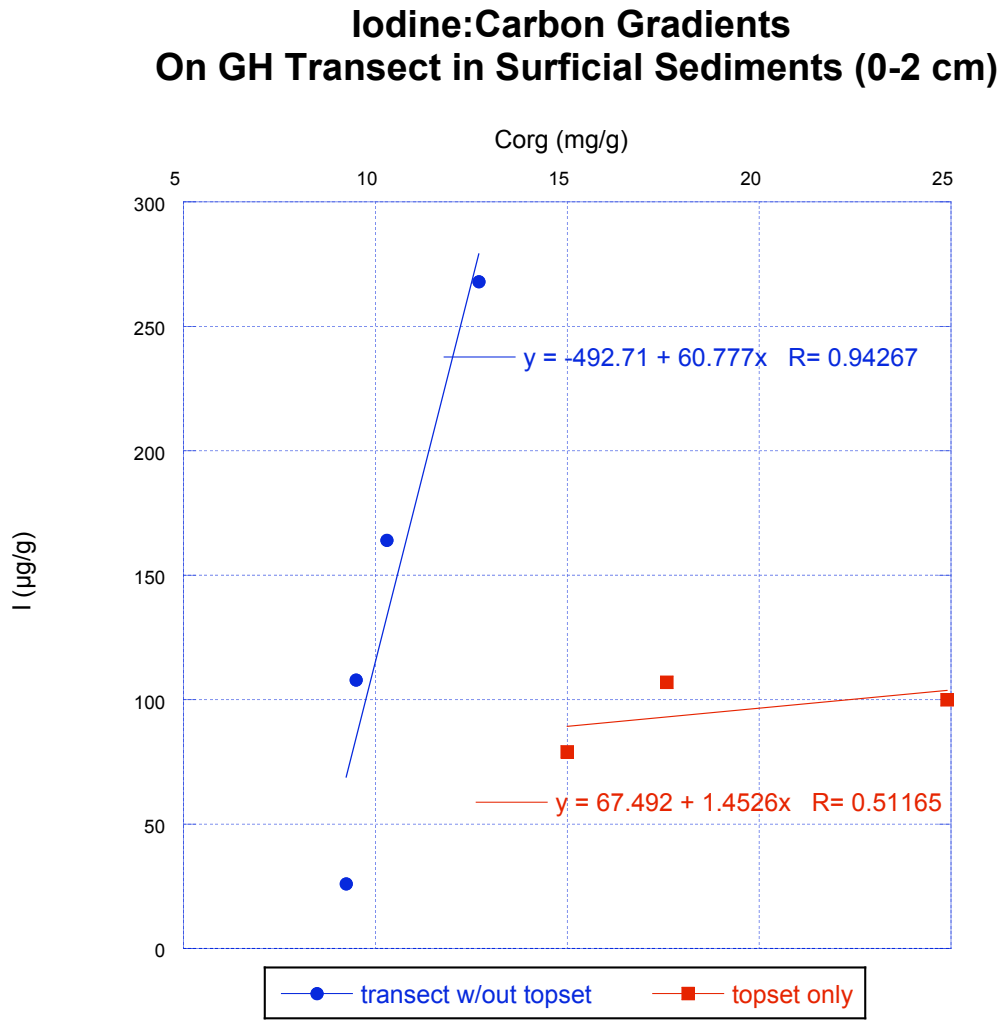

Fig 3 (a) Depth profiles of solid-phase iodine from kasten cores from topset (GH14) & foreset (GH50) sites (2003 monsoon). Solid-phase iodine profiles reflect higher offshore iodine concentrations. At GH14, iodine is apparently refractory starting at 30 - 40 cm; at GH50, profile indicates continuing solid-phase iodine loss over entire depth-scale.

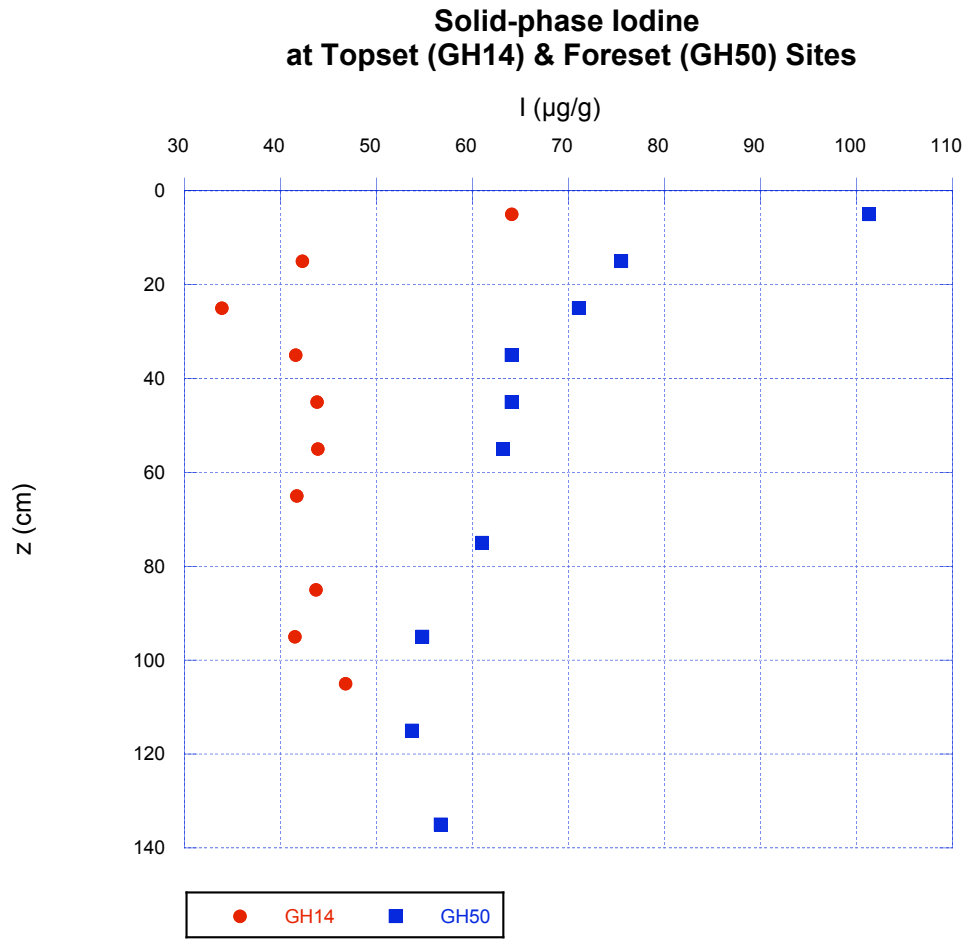

3 (b). Depth profiles of solid-phase I:C ratios from kasten cores from topset (GH14) & foreset (GH50) sites (2003 monsoon). I:C ratios reflect preferential

loss of iodine relative to C with depth at each core. At GH14, I:C ratios reflect earlier remobilization of solid-phase iodine whereas at GH50 preferential loss occurs gradually.

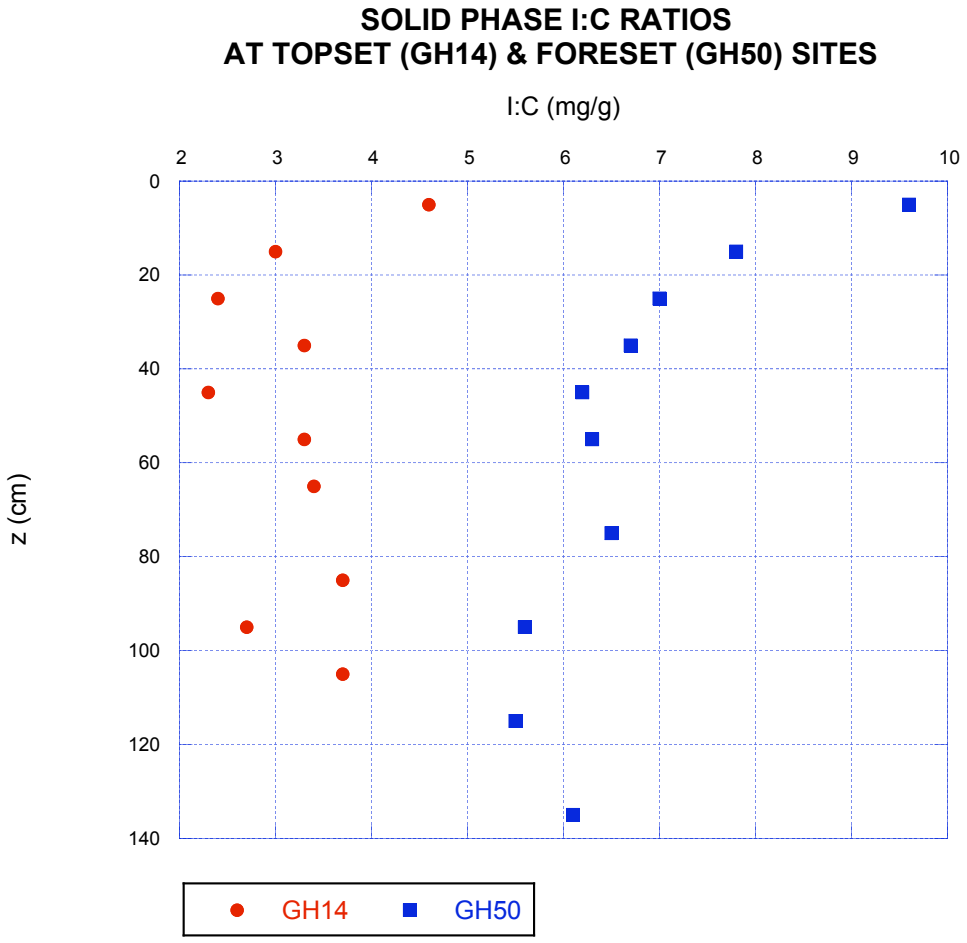

4 (a). Solid-phase iodine from piston core at GH14 (2004 monsoon)

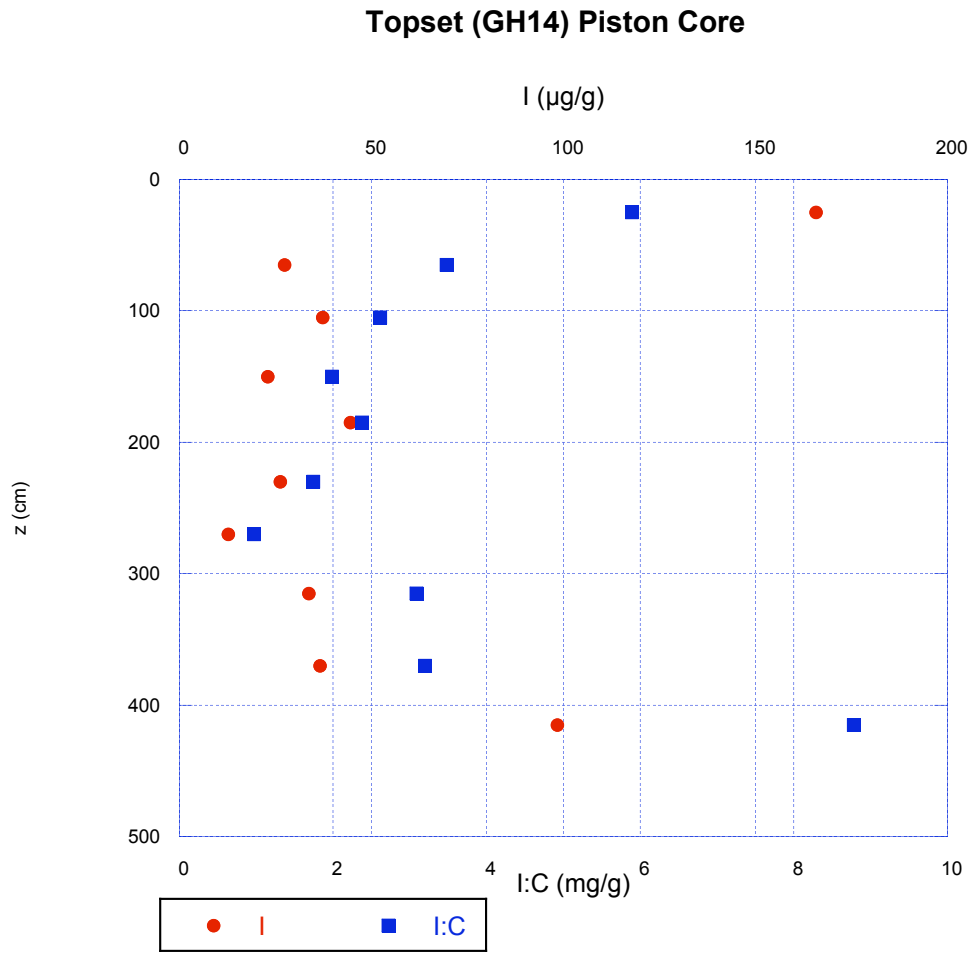

4 (b). Solid-phase iodine from piston core at GH35 (May 2004)

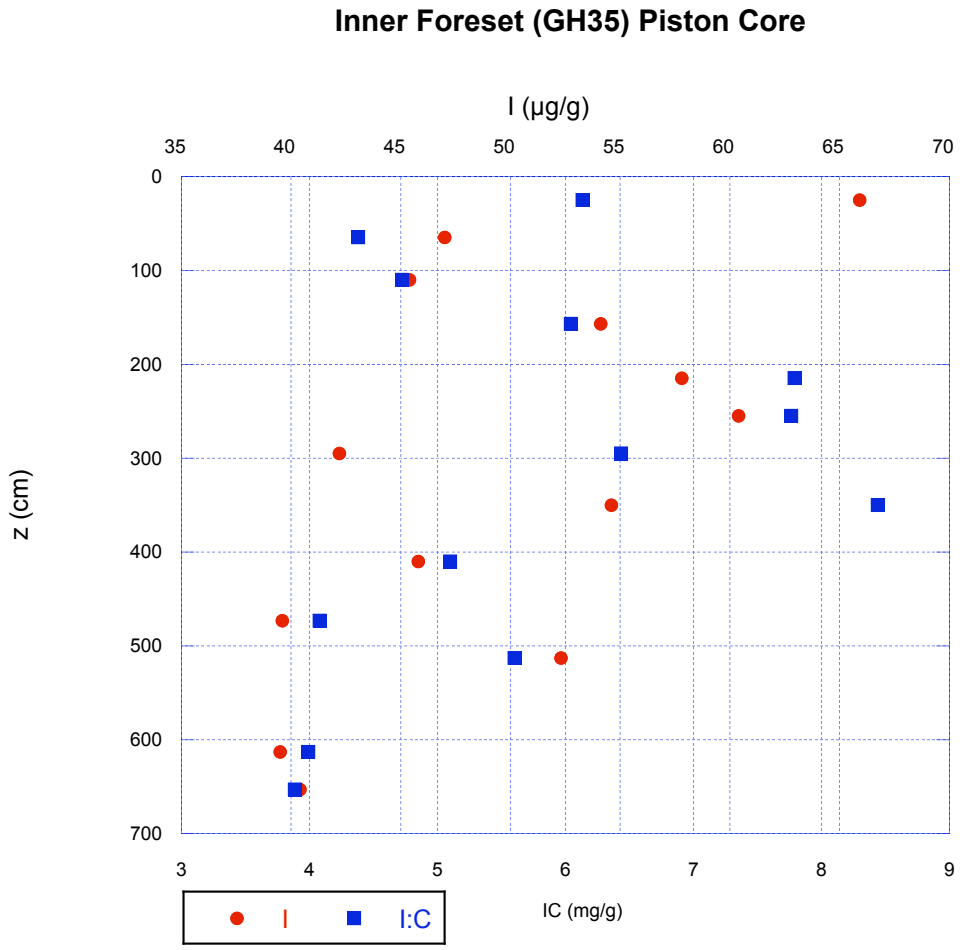

4 (c). Solid-phase iodine from piston core at GH50 (Sep 2003)

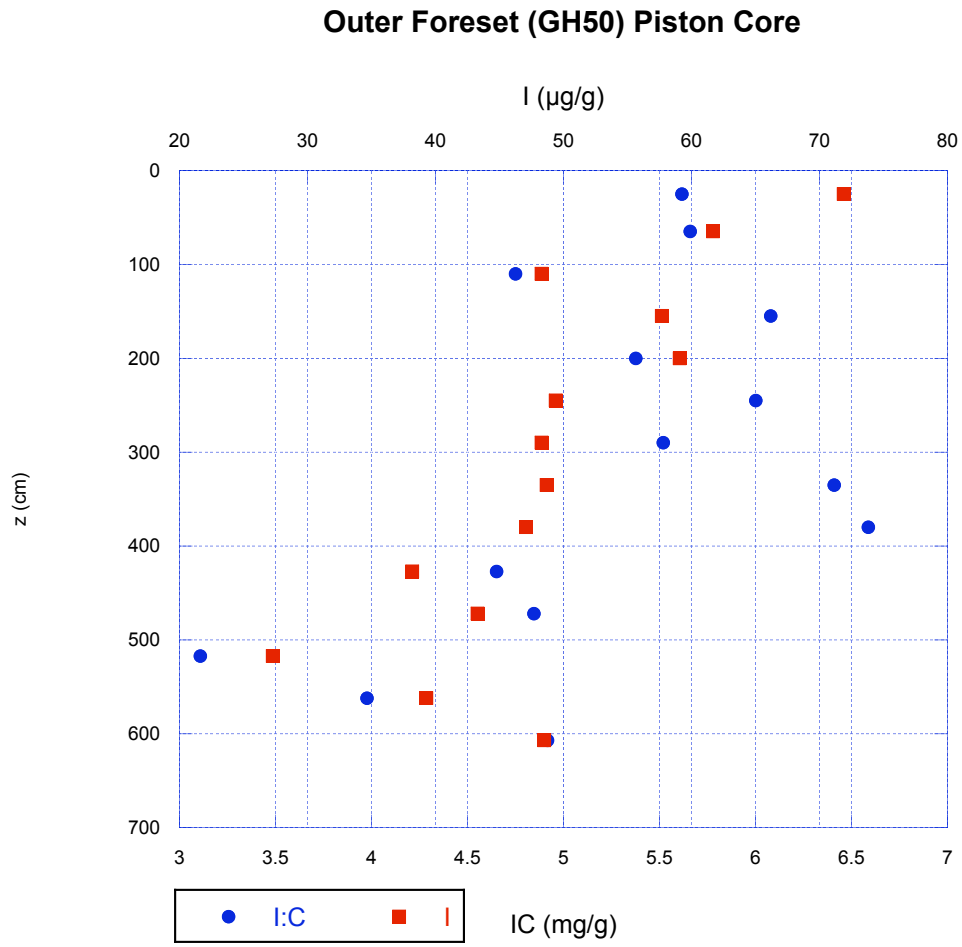

Fig 5. Dissolved iodine in porewater from short cores of sediments from GH Transect. Sampled 2003 Monsoons except for GH8 sampled Nov 2003.

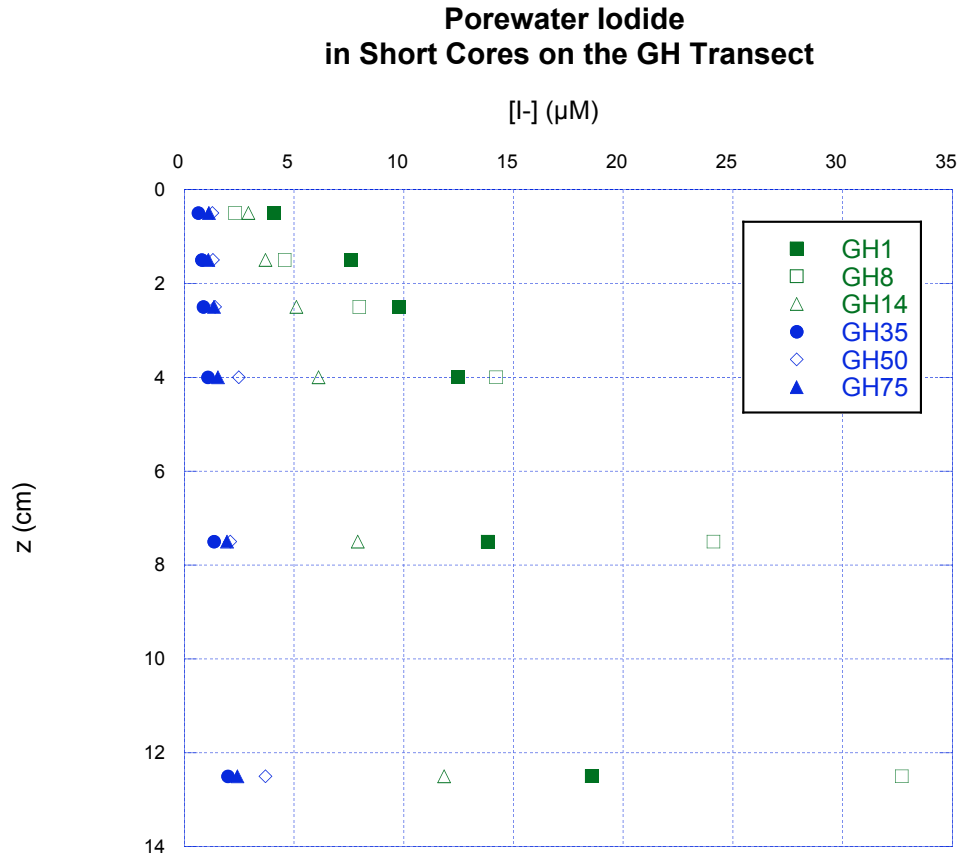

Fig 6(a). Porewater iodide profiles from kasten cores at foreset and bottomset sites . Sampled 2003 monsoons.

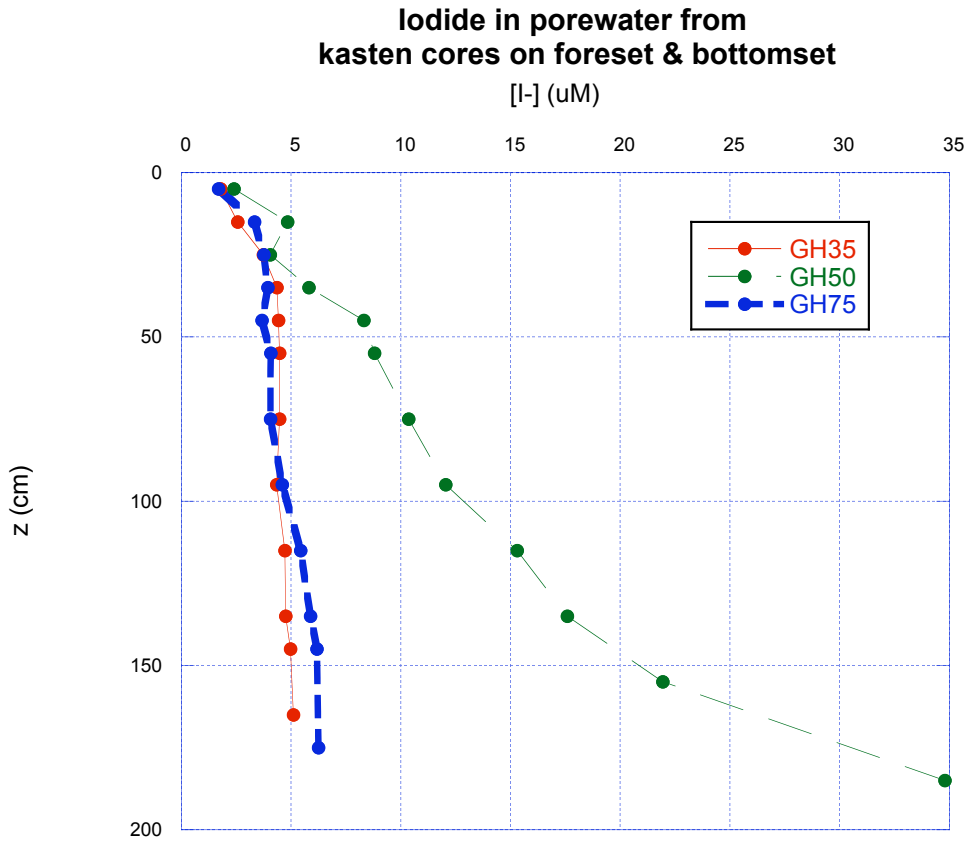

6 (b). Porewater iodide profiles from kasten cores at topset sites. Profiles show maxima & minima features in constant ^{210} Pb zone.

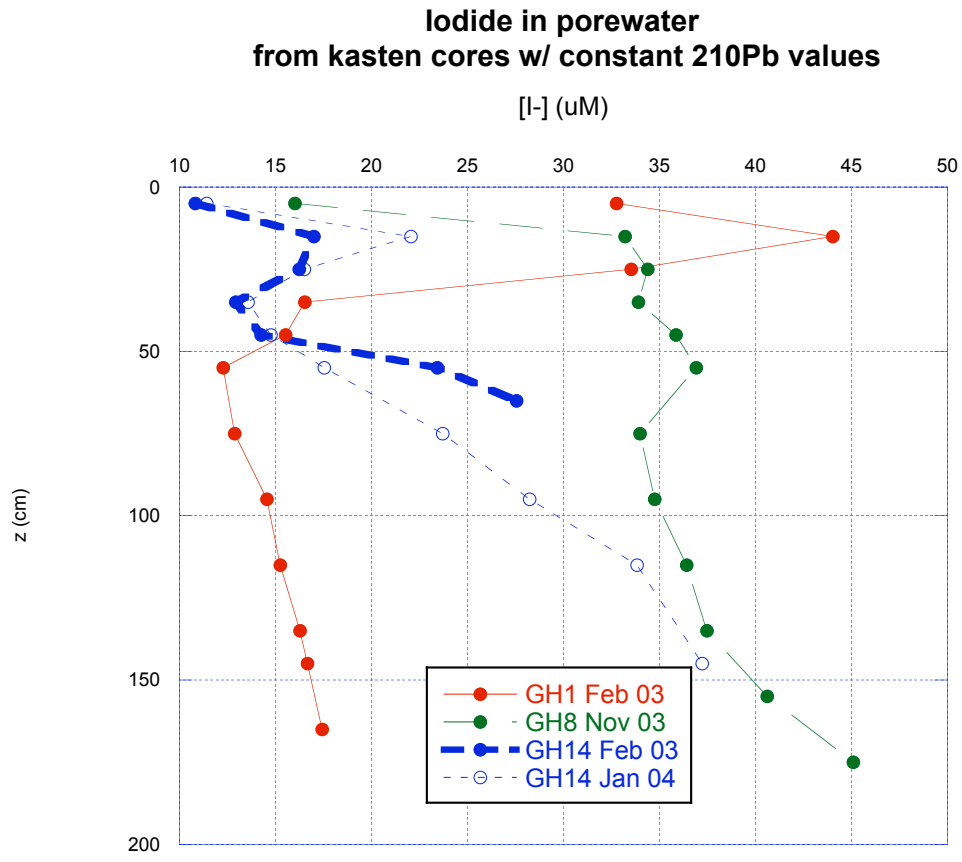

7 (a). Porewater iodide in piston cores across the GH transect.

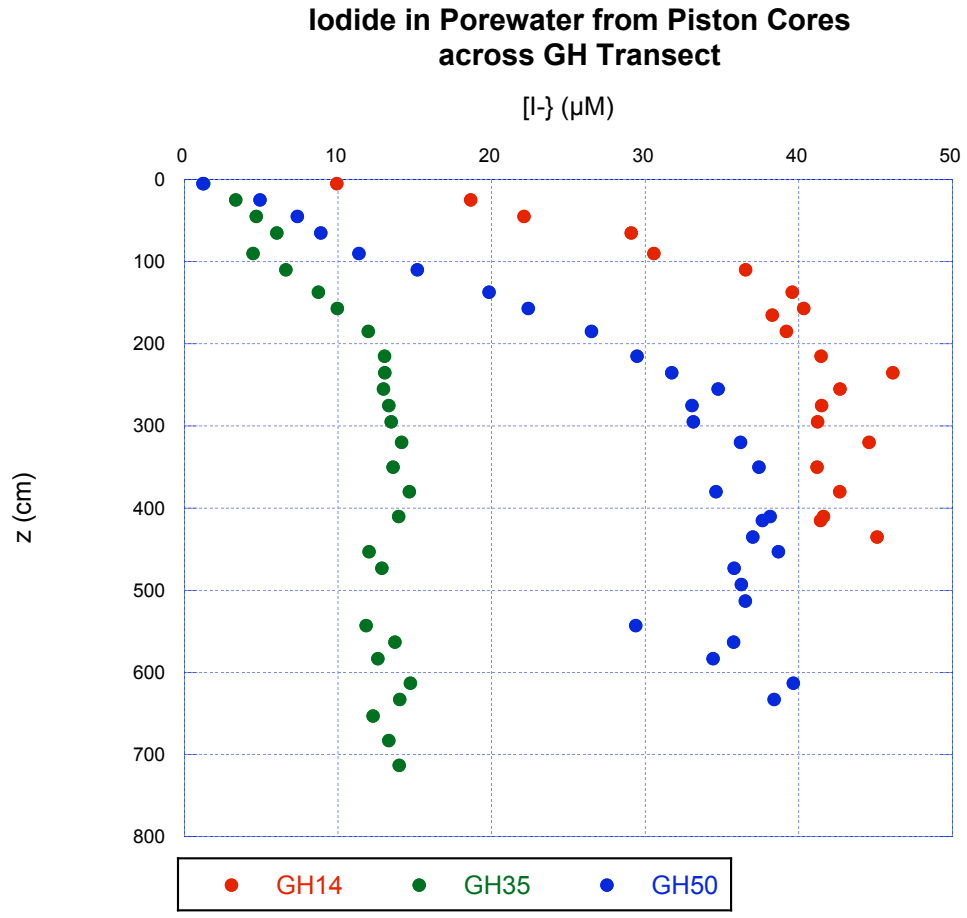

7 (b). Porewater iodide from piston core in the Umuda Valley.

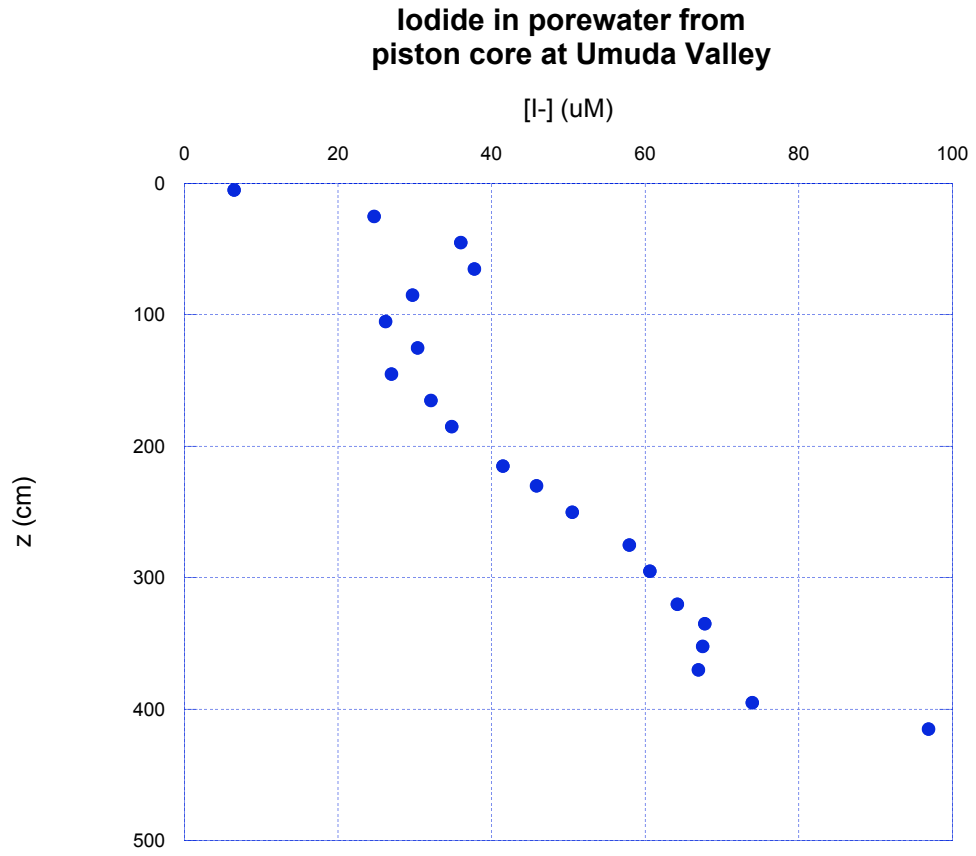

8 (a). Solute depth profiles at GH1 (mangrove channel). Iodide and dissolved Fe show maxima & minima at the same depth intervals in the constant ^{210} Pb zone and little correlation with growth in ΔCO_2. Iodide concentrations begin to increase with ΔCO_2 below the constant ^{210} Pb zone.

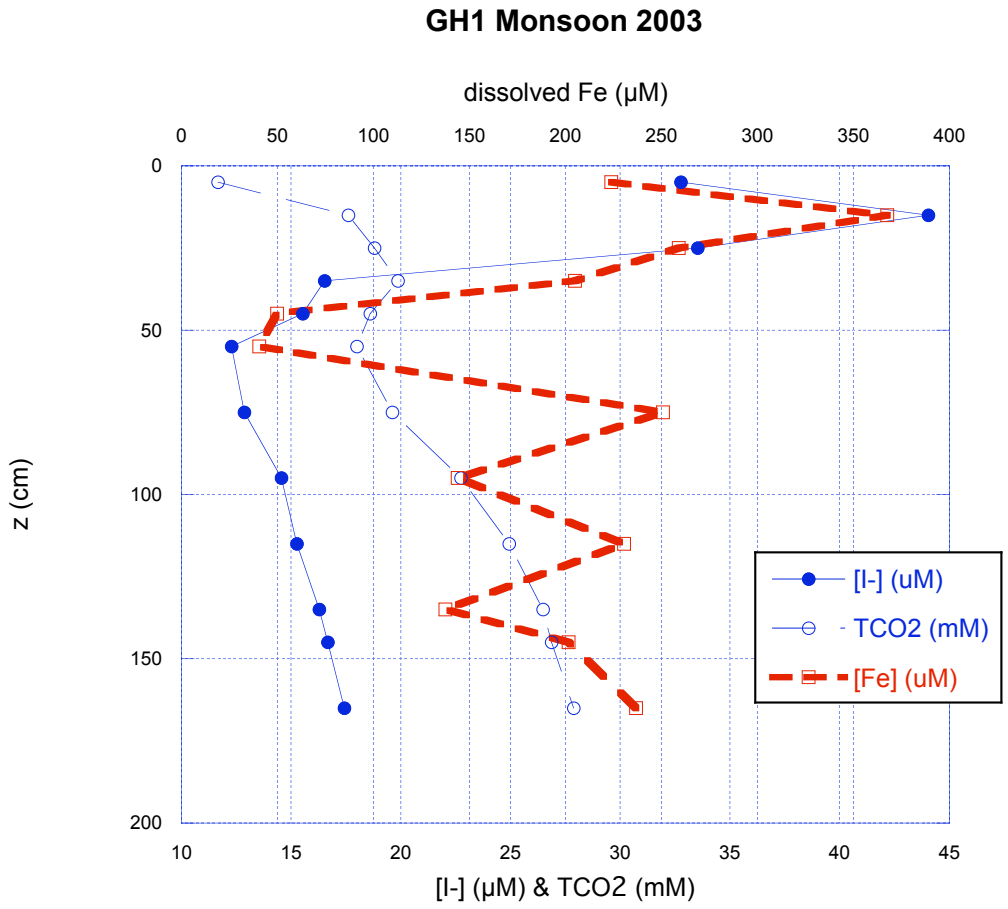

Fig 8(b). Solute depth profiles at GH8.

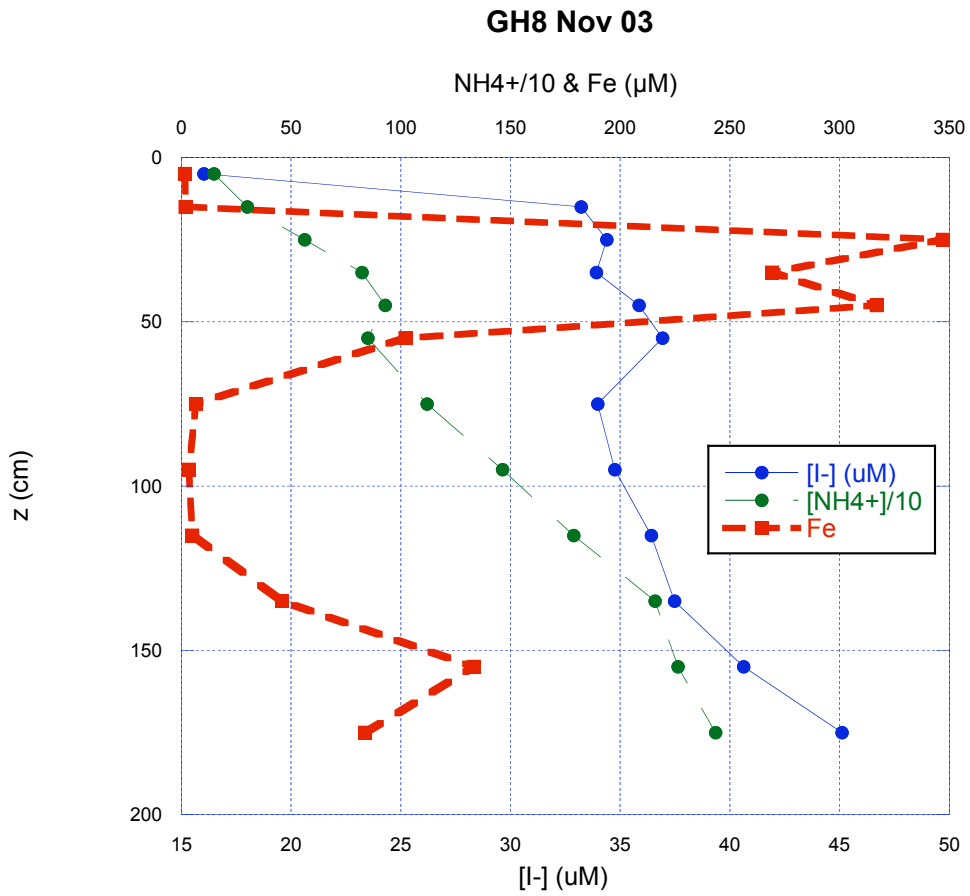

Fig 8(c). Solute depth profiles at GH50. Profiles are typical of profiles at other foreset & bottomset sites. Iodide shows a general increase with $\square CO_2$ and NH_4^+ and no relationship with dissolved Fe.

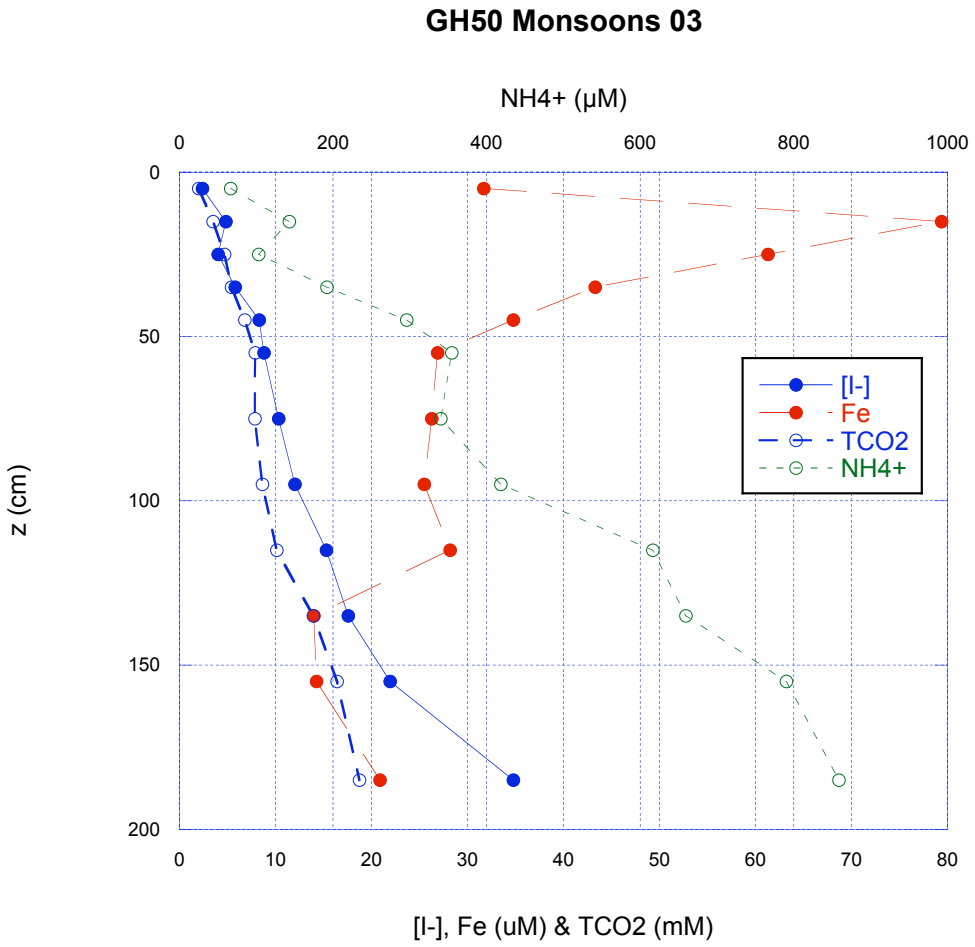

Fig 9. A comparison of porewater I:N ratios from kasten cores on the topset and foreset/bottomset. Porewater I:N ratios from kasten cores show a linear relationship with a steep trajectory across the GH transect except on the topset where I:N ratio appears trendless.

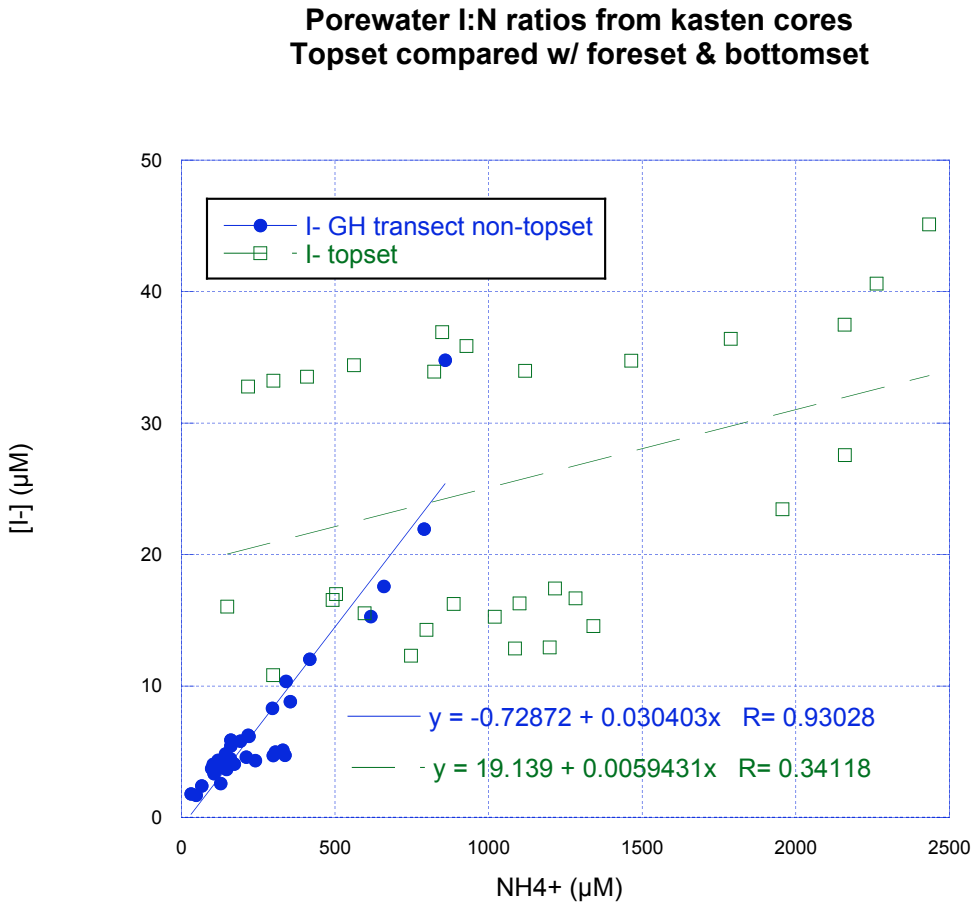

10 (a). Solid-phase iodine profiles from kasten cores on the topset (GH14) during monsoons and after SE tradewinds.

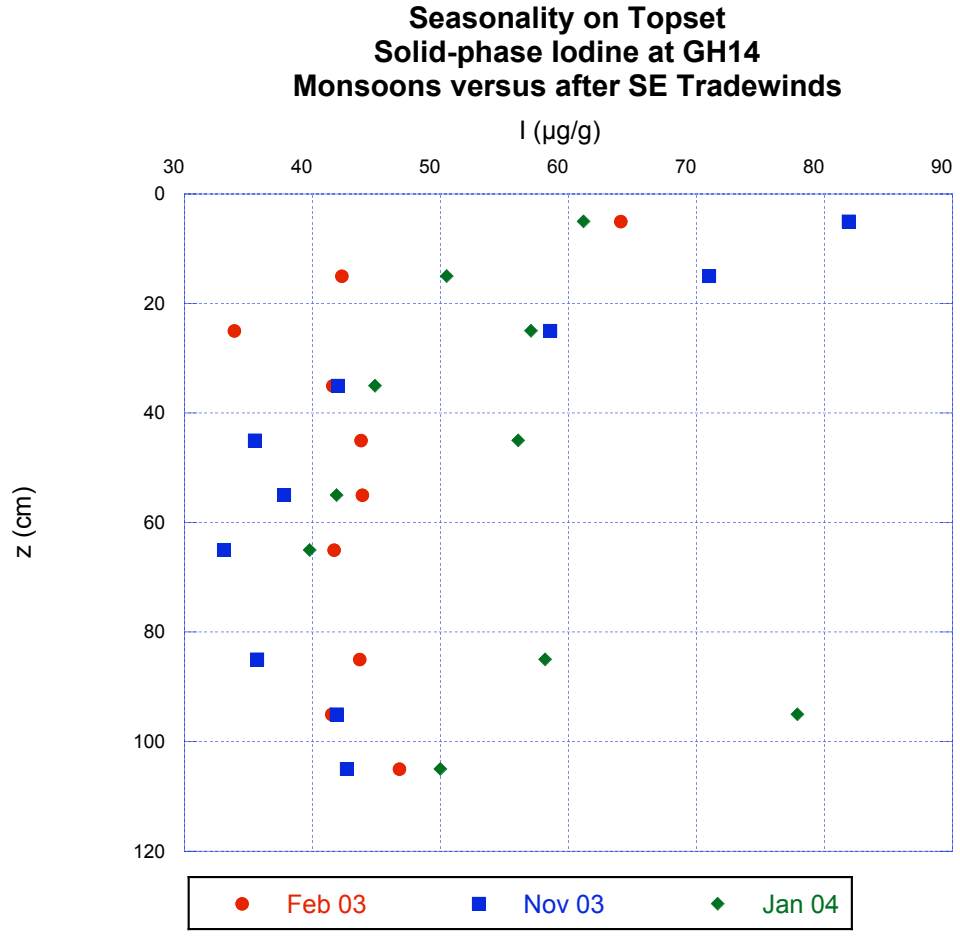

Fig 10 (b). Solid-phase iodine profiles from kasten cores on the outer foreset (GH50) during monsoon and after SE tradewinds.

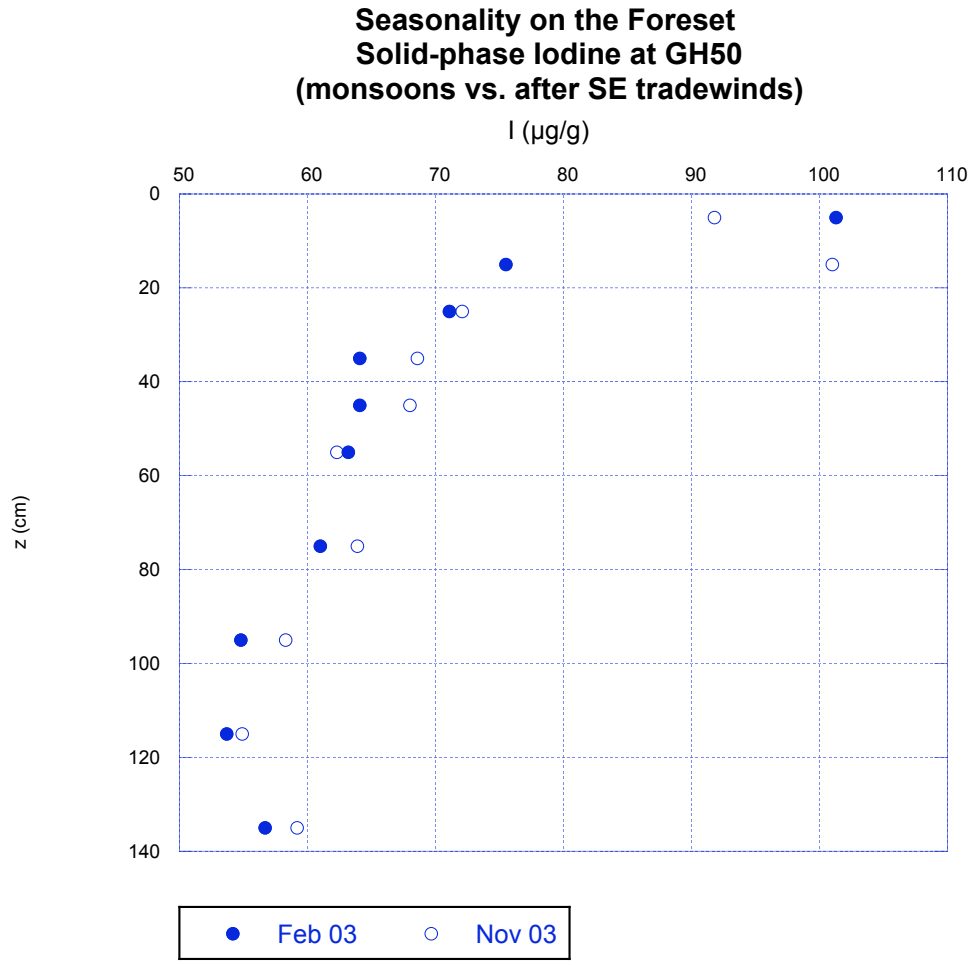

Fig 10 (c). Porewater iodide from kasten cores on the topset (GH14) during monsoons and after SE tradewinds.

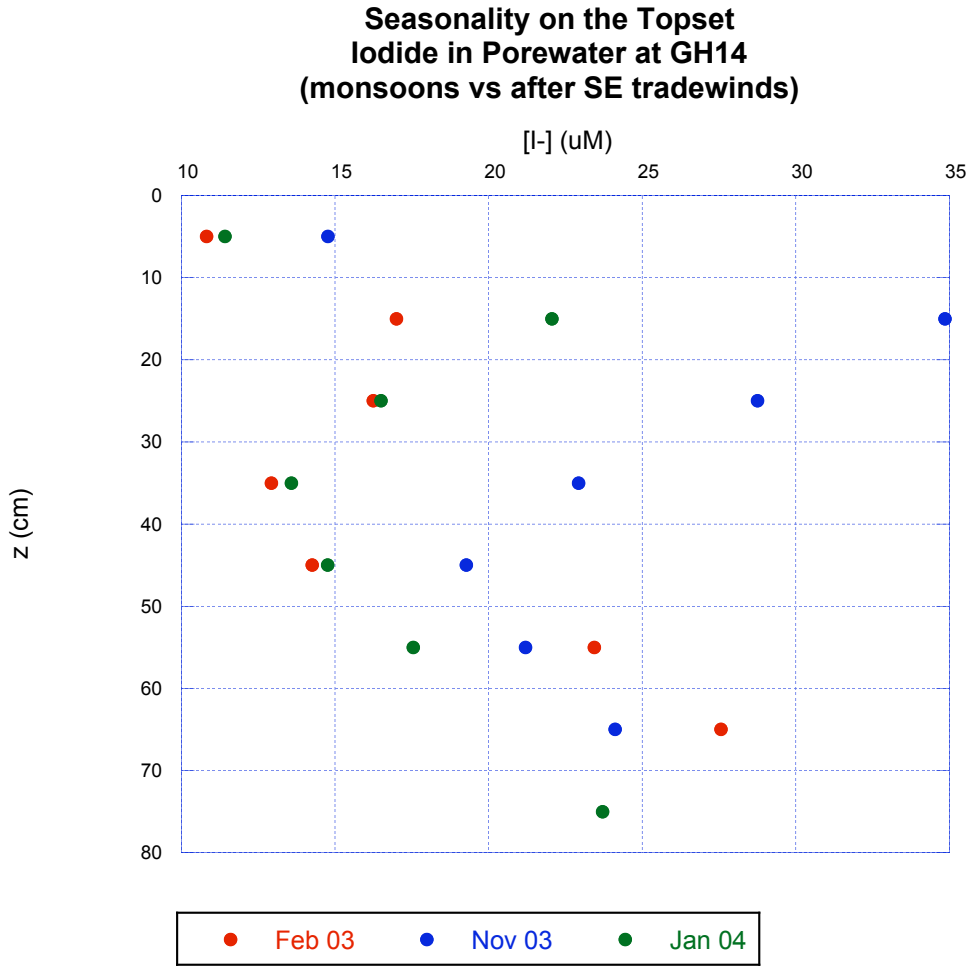

Fig 10(d) Porewater iodide profiles from kasten cores on the foreset during monsoon and after SE tradewinds

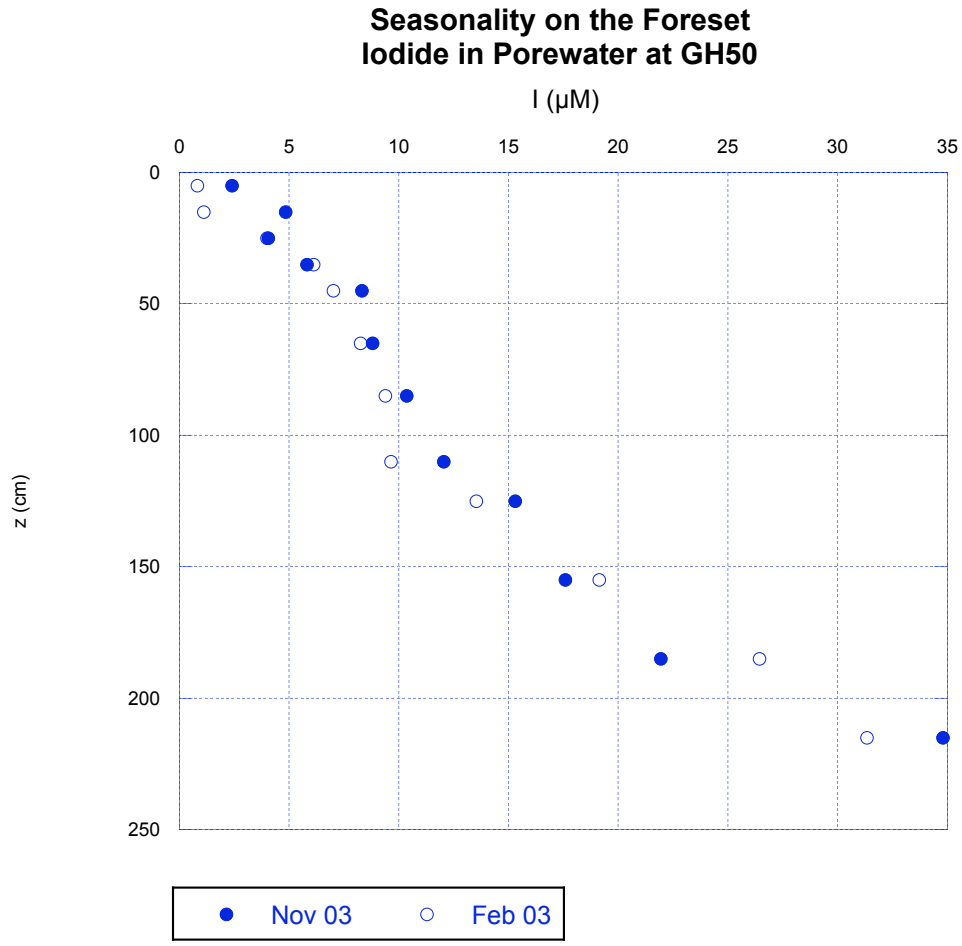

Table 1. Distribution of iodine in earth's crust.		
	PPB	%
Earth's Crust	295	
Continental	119	30.4
Oceanic	777	69.6
Oceanic Crust		
Seawater	50	0.8
Sediment	14,750	68.2
Mafic Flows	9	0.6
(1) Muramatsu & Wedepohl (1998)		

Table 2. Biophilic nature of iodine

	Concentration (wt%)	Ref.
Iodine		
Metamorphic & Magmatic rock	10's PPB	1
Sediment	0.1 - 100's PPM	1
Organic Matter:		
Higher Plants	50 - 500 PPB	2
Brown Algae	87 - 490 PPM	1
Red Algae	44 - 100 PPM	1
Faecal pellets (sed. traps)	83 - 496 PPM	3
Freshwater Fish	60 - 220 PPB	2
Marine Fish	0.5 - 6 PPM	2
Phytoplankton	(wt)	
I:C Ratio	1 mg I/ g C	1
I:N Ratio	7 mg I/ g N	1

(1) Muramatsu & Wedepohl (1998); (2) Whitehead (1984); (3) Elderfield & Truesdale (1980)

Table 3. Reported iodine concentrations in surficial sediments.			
	I (PPM)	I:C	Source:
Barents Sea	60-828	□30	Price et al 1970
Namibian Shelf	□ 750 □ 250	□25(edge) □ 2 (inner)	Price & Calvert 1973
Loch Duich	322-498	6.3 – 8.5	Krom & Sholkovitz 1977
Loch Beg	136-232	2.1 – 3.7	Krom & Sholkovitz 1977
Panama Basin	76-861	39.5	Pedersen & Price 1980
Mud Bay (S.C.)	40-60	□ 1 - 5	Ullman & Aller 1983
L.I.S.	□ 70	□ 5	Ullman & Aller 1983
Florida Bay	□ 3	□ 1	Ullman & Aller 1983
Eastern Pacific	13 - 25	3.3 – 6.5	Wakefield & Elderfield 1985
No. Atlantic	□54 - 91	□22 - 32	Kennedy & Elderfield 198
Amazon Delta	20 - 50	4 - 8	Mackin et al 1988

Table 4. Solid-phase iodine; I:C & I:N ratios in surficial sediments (upper 2 cm). Sampled during the monsoons except * (Nov 2003).

	C_{org} (mg/g)	N (□g/g)	I (□g/g)	I:C (mg/g)	I:N (mg/g)	□$^{13}C_{org}$
Fly River	9.2		26	2.8		-26.9
GH1	24.9	1.6	100	4.0	62.7	-27.6
GH8 *	15.0	1.5	79	5.3	54.1	-26.8
GH14	17.6	1.3	107	6.1	82.2	-27.0
GH35	9.5	1.1	108	11.4	102.8	-25.9
GH50	10.3	1.3	164	15.9	122.8	-25.6
GH75	12.7	1.6	268	21.2	171.6	-23.7

Table 5. A comparison of solid-phase iodine concentrations & I:C ratios in near- & offshore sediments.			
Near-shore:			
	I (μg/g)	I/C (mg/g)	Source
Gulf Topset	79 - 107	≈ 4 - 6	Present study
Namibian shelf Near-shore	≈ 250	≈ 2	Price & Calvert (1973)
Loch Beg Near-shore	136 - 232	≈ 2 - 4	Krom & Sholkovitz (1977)
Long Island Sound	≈ 70	≈ 5	Ullman & Aller (1983)
Amazon shelf	20 - 50	4 - 8	Mackin et al., (1988)
Offshore:			
Gulf Bottomset	268	≈ 21	Present study
Namibian shelf Outer shelf edge	≈ 750	≈ 25	Price & Calvert (1973)
Loch Duich Basin- marine	322 - 498	≈ 6 - 9	Krom & Sholkovitz 1977
Panama Basin	76 - 861	39.5	Pedersen & Price 1980

Table 6. Maximum concentrations of iodide in porewater.		
	$[I^-]_{max}$(□M)	Source
No. Atlantic	□ 2	Wakefield & Elderfield 1985
Mud Bay (S.C.)	□ 4	Ullman & Aller 1983
Panama Basin	9.2	Pedersen & Price 1980
Gulf bottomset	< 40	Present study
Gulf Topset	□ 45	Present study
Amazon shelf	□ 30 - 120	Mackin et al 1988

Table 7. Production estimates from solid-phase iodine concentration gradients and from incubations. Cores sampled during the monsoon period in Feb 2003 except at GH8 sampled Nov 2003. Ranges are reported where uncertainty surrounds estimation of sediment accumulation rates. (NA- not available; NR- nor reported). Particle mixing term integrated over 4 cm.

	Estimates from solid-phase iodine concentration gradients					Estimates from incubations	
Short Cores	R_0 (mmol cm^{-3} d^{-1})	β cm^{-1}	D_B (cm^2 yr^{-1})	α (cm yr^{-1})	Flux (μmol m^{-2} d^{-1})	t=1 (μmol $m^{-2}d^{-1}$)	t=2 (μmol m^{-2} d^{-1})
GH1	.0562	0.6701	NA	12.0	NR	354	112
GH8	NR	NR	NA	NA	NR	90	NA
GH14 low	.0031	0.7258	NA	0.7	10	33	24
GH14 high	.0088	0.7258	NA	2.0	26		
GH35 low	.0030	0.6145	NA	1.4	11	63	20
GH35 high	.0095	0.6145	NA	4.4	34		
GH50	.0023	0.2400	.0031	1.7	33	15	33
GH75	.0028	.1193	.0010	0.56	24	71	44

Table 8. Comparison of production estimates of I^{-1} , ΔCO_2 & NH_4^+. Note: All amounts are from t=1 incubations for depths to 15 cm except for (1) ΔCO2 at the GH75 site which is from a t=2 incubation to 15 cm and (2) I at the GH50 site which is the flux number derived from the solid-phase concentration gradient over the upper 15 cm.

	ΔCO_2 mmol/m2-d	NH_4^+ mmol/m2-d	Iodide μmol/m^2-d	I:C mmol/mol	I:N mmol/mol	Implied C:N
GH1	31.2	8.21	354	11.3	43.1	3.8
GH8	16.1	0.986	90.0	5.6	91.3	16.3
GH14	14.9	4.05	33.2	2.2	8.2	3.7
GH35	23.5	5.74	63.4	2.7	11.0	4.1
GH50	10.7	1.44	32.6	3.0	22.6	7.5
GH75	6.3	2.85	71.2	11.3	25.0	2.2

Table 9. Iodide production estimates from porewater iodide concentrations in piston cores. GH14 (sampled Jan 2004); GH35 (May 2004) & GH50 (Sep 2003). Ranges are reported where uncertainty surrounds estimation of sediment accumulation rates.

	ϕ (cm^{-1})	D_s ($cm^2\ d^{-1}$)	ω ($cm\ yr^{-1}$)	Flux ($\mu mol\ m^{-2} d^{-1}$)
GH14(low)	0.0086	0.7167	0.7	2
GH14(high)	0.0086	0.7167	2.0	3
GH35(low)	0.0088	1.1175	1.4	1
GH35(high)	0.0088	1.1175	4.4	2
GH50	0.0073	1.1473	1.7	3

Table 10. Comparison of production ratios & porewater solute stoichiometric ratios (all data from 2003 monsoons except GH8(Nov 2003).				
	Incubation Data		Porewater Stoichiometric Ratios	
	I:C mmol/mol	I:N mmol/mol	I:C mmol/mol	I:N mmol/mol
GH1	11.3	43.1	1.9	69.7
GH8	5.6	91.3	5.0	94.4
GH14	2.2	8.2	1.1	33.3
GH35	2.7	11.0	non-linear	18.7
GH50	3.0	22.6	3.8	26.9
GH75	11.3	25.0	2.4	21.9

Table11. Correlation between porewater iodide and (1) $\square CO2$ & NH_4^+ and (2) dissolved Fe. From kasten cores in constant ^{210}Pb intervals for topset/Umuda Valley sites and for entire core for foreset and bottomset sites. All cores sampled 2003 monsoon except GH8 & GH14 (Trades) sampled Nov 2003; T8-18 ^{210}Pb interval (Jan 2004) & T8-18 piston (May 2004).

	Correlation Coefficients		
	I- & $\square CO_2$	I- & NH_4^+	I- & Fe
GH1	< 0	< 0	0.91
GH8	0.54	0.60	0.29
GH14 (Mons)	0.23	0.16	0.06
GH14 (Trades)	-0.05	-0.07	-0.02
T8-18 $=^{210}Pb$	< 0	< 0	0.84
T8-18 (piston core)	0.09	.89	< 0
GH35	0.95	0.76	< 0
GH50	0.96	0.94	< 0
GH75	0.96	0.86	< 0

Table12. Comparison of production during monsoon & after SE tradewinds periods on topset and outer-foreset.

		GH14	GH14	GH50	GH50
		Monsoon	After SE Trades	Monsoon	AfterSE Trades
Production (I)	μmol/m^2-d	33.2	23.4	32.6	36.1
CO_2 Production	mmol/m^2-d	14.9	11.8	10.7	11.7
NH_4^+ Production	μmol/m^2-d	4,054	1,117	1,440	2,217
I:C Product Ratio	mmol/mol	2.2	2.0	3.0	3.1
I:N Product Ratio	mmol/mol	8.2	20.9	22.6	16.3

Appendix 1. Fitted versus measured data: Reactive solid-phase iodine at GH14

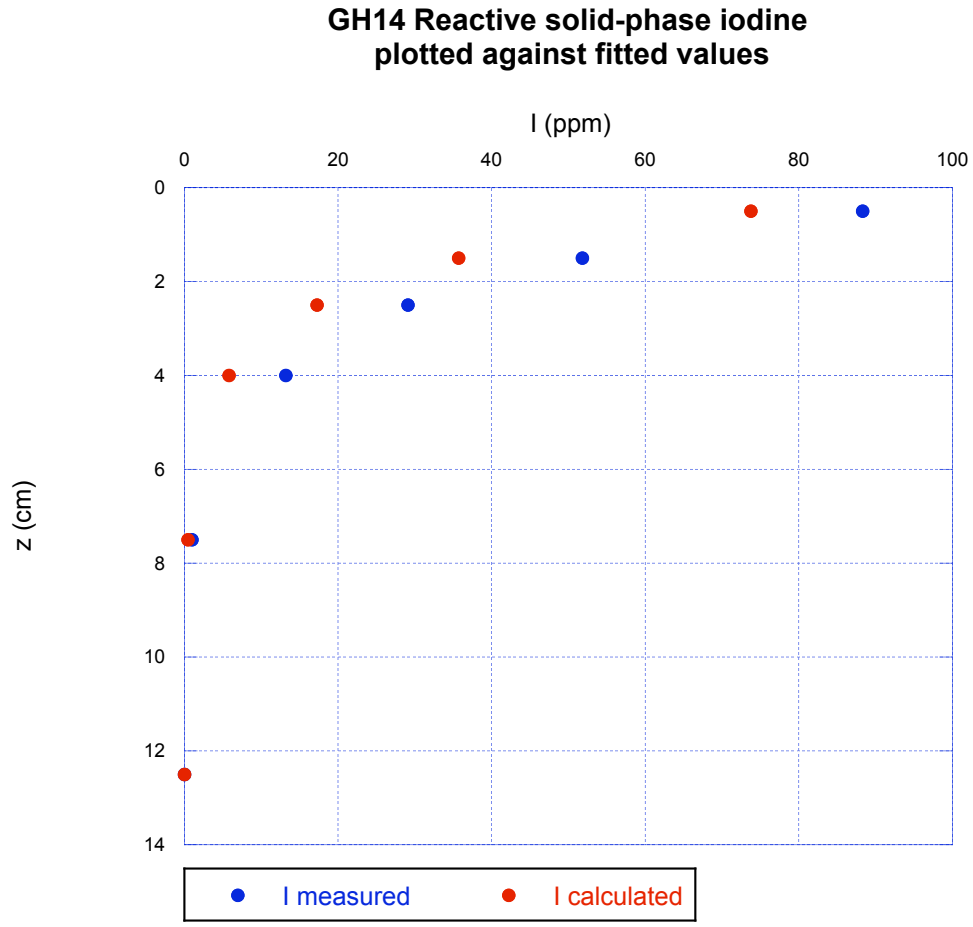

I (calc) = 106 * EXP(-.7258 * z) R^2 = 0.9839

Appendix 2. Fitted versus measured data: Reactive solid-phase iodine at GH35

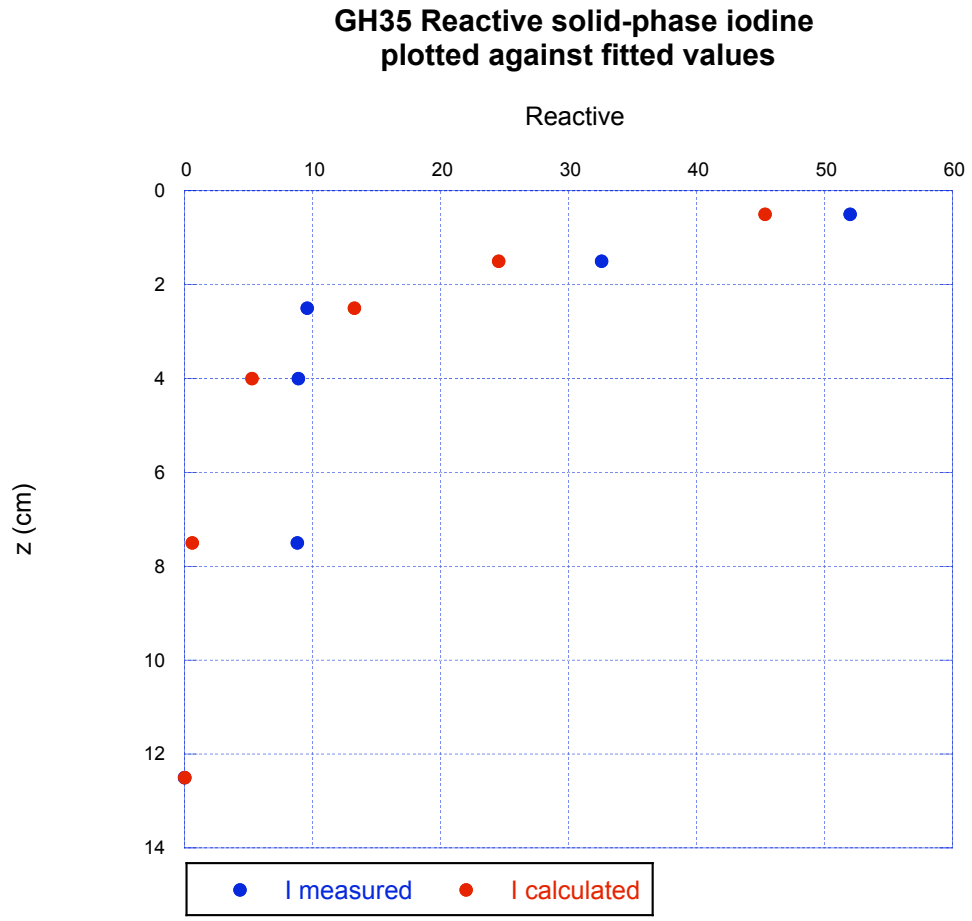

I (calc) = 61.7 * EXP (-0.6145 * z) R^2 = 0.9461

Appendix 3. Fitted versus measured data: Reactive solid-phase iodine at GH50

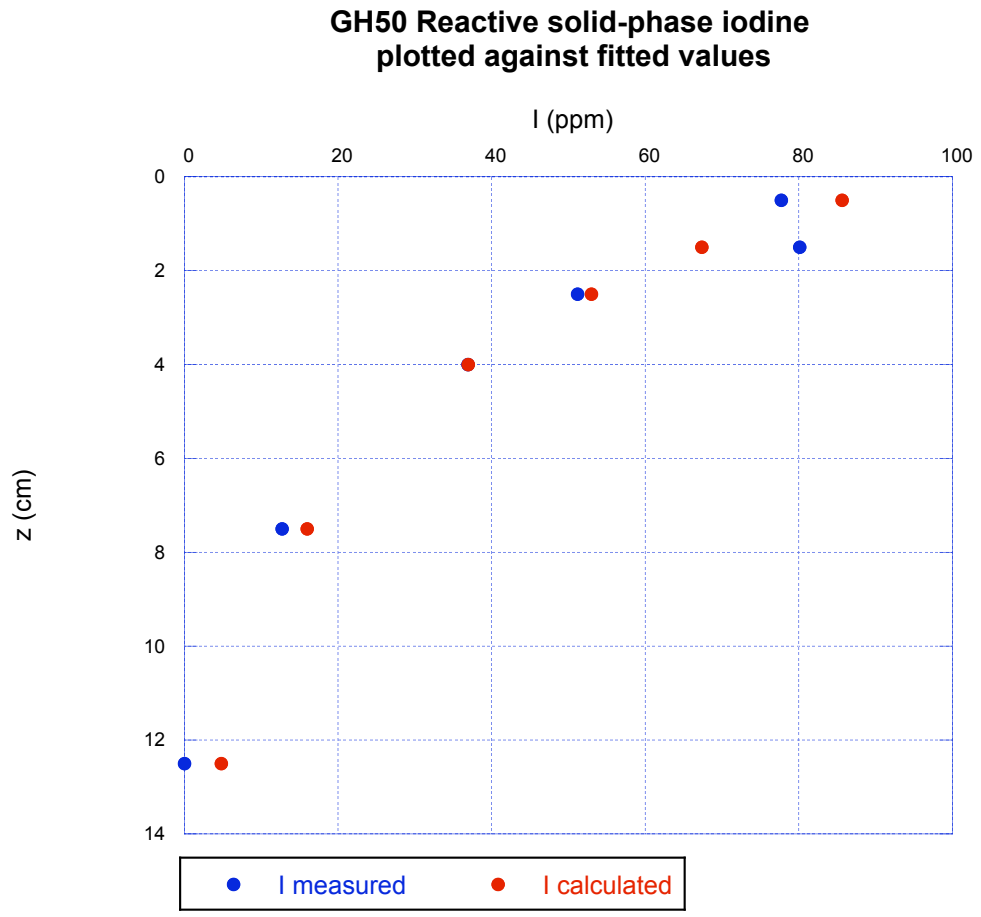

I (calc) = 96.55 * EXP (-0.24 * z) R^2 = 0.9548

Appendix 4. Fitted versus measured data: Reactive solid-phase iodine at GH75

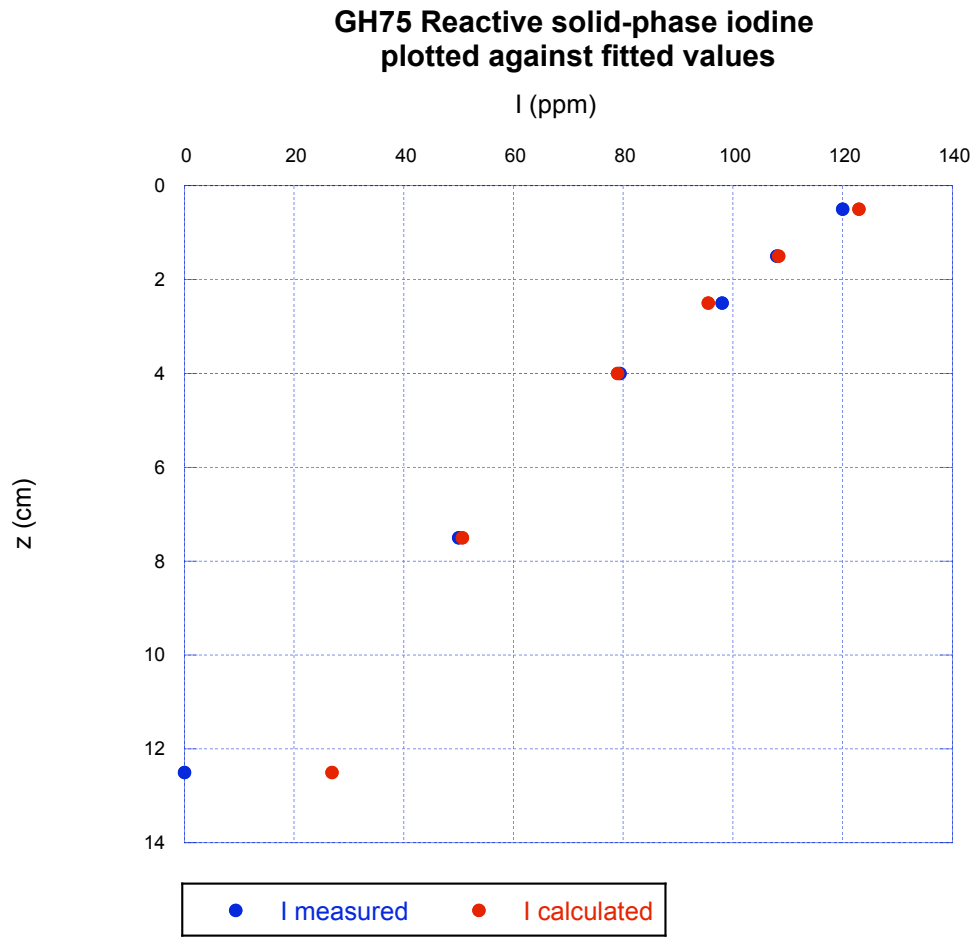

I (calc) = 126 * EXP (-0.1193 * z) R^2 = 0.9708

Appendix 5. Fitted versus measured data: Porewater iodide at GH14.

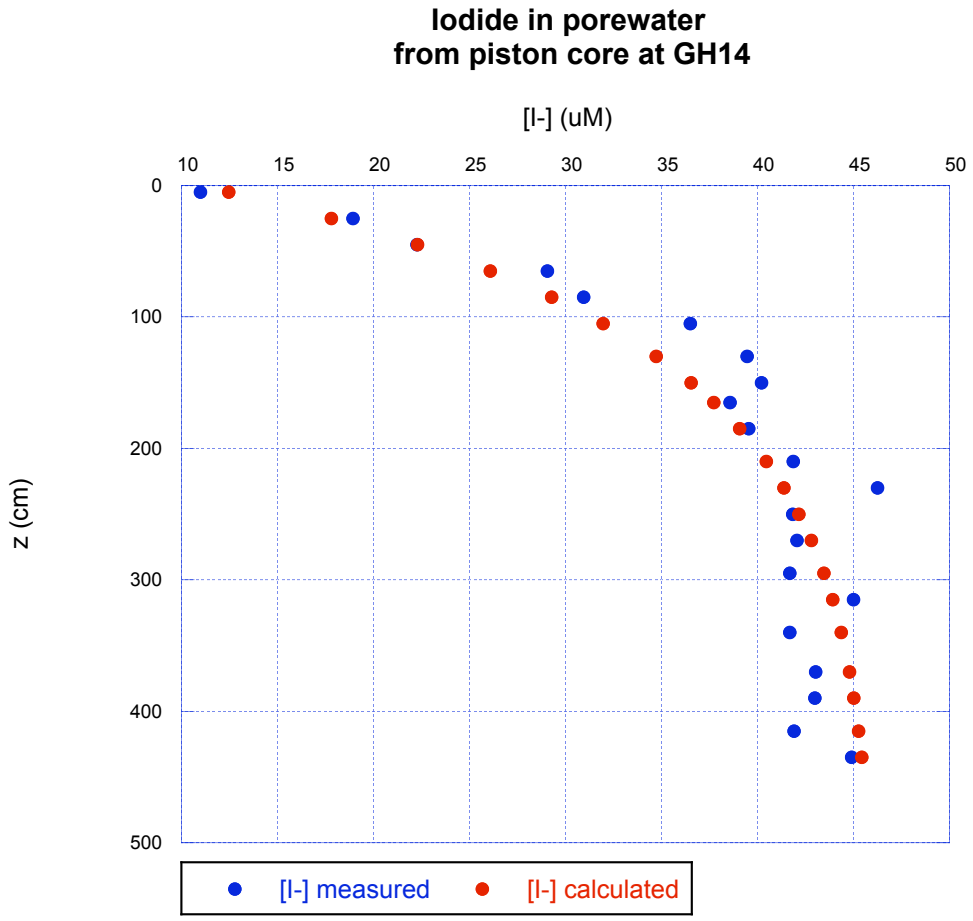

I (calc) = 10.98 + 35.28 * (1 – EXP(-.0086 * z)) R^2 = 0.9116

Appendix 6. Fitted versus measured data: Porewater iodide at GH35.

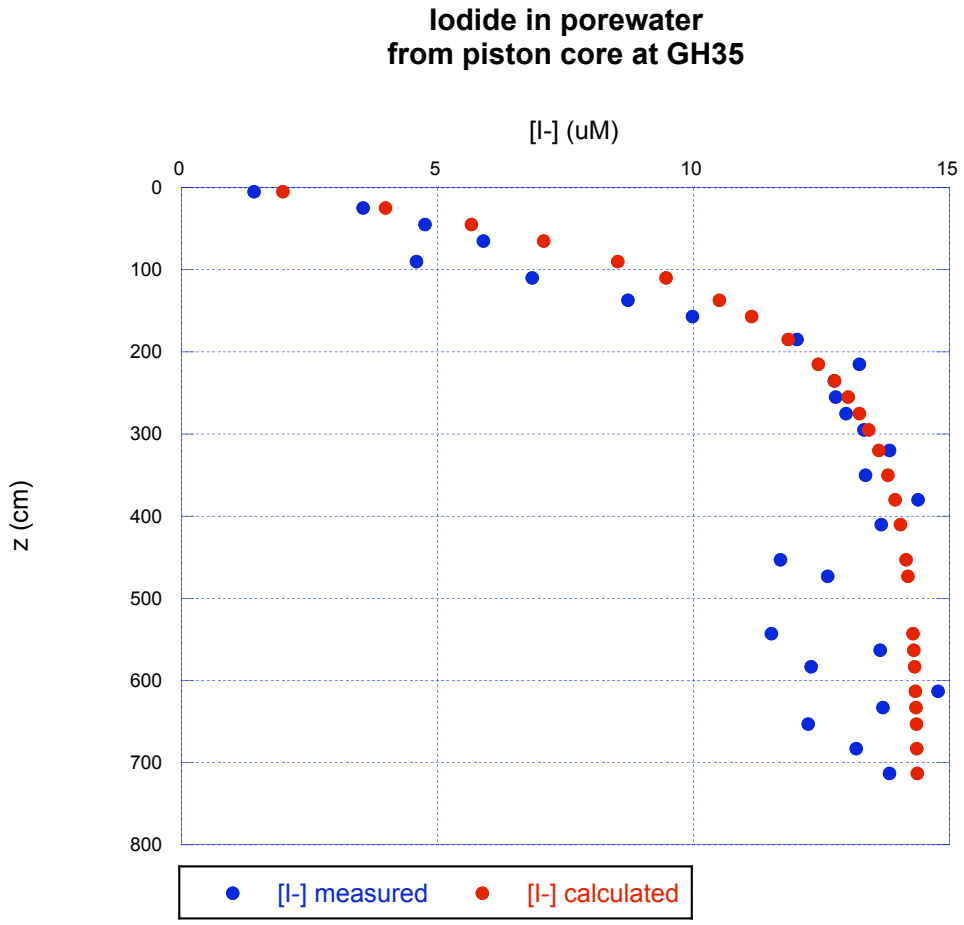

I (calc) = 1.42 + 12.97 * (1 – EXP(-.0088 * z)) R^2 = 0.9089

Appendix 7. Fitted versus measured data: Porewater iodide at GH50.

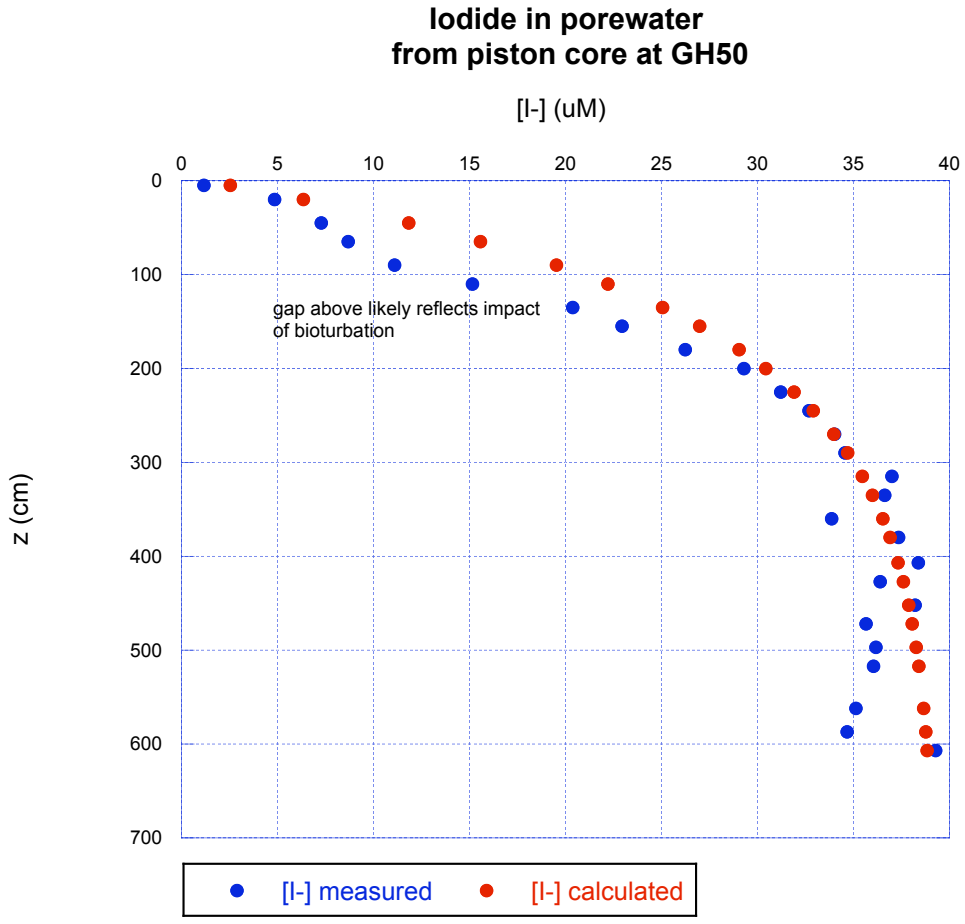

I (calc) = 1.177 + 38.11 * (1 – EXP(-.0073 * z)) R^2 = 0.9613